UCSD-SP-68-3

PENETRATION OF SOLAR PROTONS TO FOUR EARTH RADII IN THE EQUATORIAL PLANE

NSG-538

R. Walker Fillius

Department of Physics
University of California, San Diego
La Jolla, California 92037

March 1968

Presented at the IAGA Commission V, Solar-Terrestrial and Cosmic-Terrestrial Relationship Conference, St. Gall, Switzerland, September 1967.

Penetration of Solar Protons to Four Earth Radii in the Equatorial Plane

R. Walker Fillius

University of California, San Diego

La Jolla, California, U.S.A.

ABSTRACT

On February 5, 1965, March 24, 1966, July 7, 1966, August 28, 1966, and September 2, 1966, solar protons in the 40 to several hundred MeV range were monitored by satellite Explorer 26 at low L values inside the boundary of trapped radiation near the geomagnetic equator. The arrival of particles was prompt whenever the satellite was in a position to see them. The arrival of the February 5 protons occurred 60 ± 12 minutes after the flare was observed; the March 24, 1966 protons arrived 38 ± 3 minutes after the flare; and the August 28, 1966 protons 66 ± 5 minutes after the flare. The March event was seen simultaneously by Vela 2A and 2B, and by OGO-I outside the magnetosphere. The arrival, intensity, and time profiles at the different spacecraft are comparable. Following the event of September 2, 1966, solar protons between 40 and 250 MeV were present for several days. The peak flux of 4500 ± 500 cm^{-2} sec^{-1} at 1540 UT and the decay time constant of about 8 2/3 hours correspond closely with simultaneous measurements made by satellites 1963-38C and 1966-70A

Presented at the IAGA Commission V, Solar-Terrestrial and Cosmic Terrestrial Relationship Conference, St. Gall, Switzerland, September 1967.

above the polar caps. The spatial distribution was characterized by a plateau of constant intensity equal to that seen over the polar caps, bordered by a region of east-west asymmetry below the particle cutoffs for some directions of arrival, terminated by the final cutoffs for eastbound particles. The cutoffs are below their classical Störmer values, but they are ~~satisfactorily~~ empirically described by a modified Störmer theory. The cutoff altitudes are lowered during the magnetic storm, and our limited sample correlates better with K_p than with D_{st}. It can be shown that a symmetrical ring current is expected to raise the equatorial cutoffs, so that some other mechanism is needed to account for the storm effect. The geomagnetic tail may account for this mechanism. The particles seen in these events show no evidence for merging with the trapped radiation and becoming permanently trapped.

I. INTRODUCTION

Most observations of solar flare produced protons have been restricted to high latitudes near the earth's surface or to interplanetary space outside the magnetosphere. Ground stations, balloons, and low altitude polar orbiting satellites have been used to investigate a wide variety of effects concerning the entry and motion of those particles in the terrestrial field, their time dependence, the position of their latitude cutoffs, and the possibility of permanent trapping. In this paper we report > 40 MeV solar protons observed by satellite Explorer 26 at altitudes of 3-5 earth radii inside the magnetosphere near the geomagnetic equator. Events in whch solar protons were monitored are those of February 5, 1965, March 24, 1966, July 7, 1966, August 28, 1966, and September 2, 1966.

The arrival of solar protons over the polar caps has been well recorded on the ground by absorption and other radio techniques, with onset times typically down to an hour after a flare (Reid and Leinbach, 1959; Bailey, 1964). Direct detection of the ionizing particles by balloons and high inclination and high eccentricity satellites reveals time lags of several hours to two days for < 10 MeV particles, (Pieper, Zmuda, Bostrom, and O'Brien, 1962; Bryant, Cline, Dessai,and McDonald, 1962) an hour for > 30 MeV particles (Van Allen and Lin, 1960) and less than a half hour for $\sim$ 170 MeV protons (Arnoldy, Hoffman, Peterson, and Winckler, 1959). The arrivals at high altitudes near the equator are presented in Section IIIof this paper.

For most events the time dependence can be interpreted in terms of diffusion in interplanetary space, under the assumption that all particles are produced instantaneously by a solar flare. Intensity-time profiles obtained by Explorer 26 will be discussed in Section 5.

A consistent feature of polar cap absorption events is the uniformity of ionization across the polar cap and down to some cutoff latitude. This uniformity is seen by high-inclination satellites where it appears as a plateau of uniform particle flux when the satellite passes above the cutoff latitude for the threshold energy of a particular detector (Lin and Van Allen, 1964; Pieper, et al 1962). Directional isotropy also prevails over the upper hemisphere (Ogilvie, Bryant, and Davis, 1962; Pieper, et al, 1962). A departure from isotropy is reported in which the low energy (< 22 MeV) protons at high latitudes near the dayside cutoff had a peak in their angular distribution perpendicular to the local B vector (Paulikas, Blake, and Freden, 1968). These particles were taken to be quasi-trapped, mirroring between hemispheres and drifting to longitudes away from the injection point. During the same event Paulikas et al report that the boundary between low energy solar protons (1.1 - 1.6 MeV) and their trapped counterparts became indistinguishable. The equatorial angular distribution and cutoff profiles obtained by Explorer 26 during this event are presented in section IV. A method is shown to fit these data with a modified Störmer theory, and the distinction between trapped and non-trapped particles is investigated.

For solar protons, as well as for galactic cosmic rays, the cutoff latitudes are lower than their theoretical Störmer values, and the cause is sought in external current systems. Both the ring current and the magnetospheric boundary currents when acting alone have been found inadequate. (Akasofu, Lin, and Van Allen, 1963) Models and calculations emphasizing the combined effect of boundary and ring currents (Akasofu, et al, 1963), turbulence (Ray, 1964), and the geomagnetic tail (Reid and Sauer, 1967; Gall, Jimenez and Camacho, 1967) are still proposed. In section VI of this paper the effect of a storm on equatorial cutoffs is presented, and it is demonstrated that this is inconsistent with the effect produced by symmetrical ring and/or boundary currents.

II. INSTRUMENTATION

Explorer 26 is in a high-eccentricity, low-inclination orbit designed to monitor the trapped radiation, with apogee at 5 earth radii, perigee at .047 earth radii, and inclination 20°. Launched in December 1964 and initially spin stabilized, the satellite despun to about 2 rpm in fall, 1966, the latest period reported here. Although the spin appeared regular between perigees, the spin vector is unknown to us and there are indications that atmospheric perturbations at perigee changed it from orbit to orbit.

There are two University of California, San Diego (UCSD) detectors aboard, named A and D, each with a low and a high discrimination level, A1, A2, and D1, D2. The counts from these discriminators are fed through four-stage ungated prescalers and subcommutated onto a single encoder channel. This channel has an accumulation time of 9.2 sec. and a readout period of 17 sec., cycling through all four discriminators in 68 seconds. Thus the minimum resolving time for each discriminator is about a minute, and the recording of n events by the encoder in one accumulation interval indicates an average counting rate of $1.75\ n = 16/9.2\ n$. For much of the data considered in this paper the counting rate was below the quantization level of 1.75 c/s, with the result that the telemetry record consists of zeros interspersed with single events. In order to extend the counting rate scale downward from 1.75 these counting rates have been averaged between consecutive events, so that an interval of n readings between single counts has an average counting rate of $1.75/n$. The data in the figures which are plotted as stepped bar graphs have been treated in this manner.

We deal mainly with detector A discriminator 2 since it is able to make unambiguous identification of solar particles. This omni-directional detector consists of a spherical ball of plastic scintillator 0.4 cm in diameter centered inside a hemispherical dome and connected by a light pipe to a photomultiplier tube. The aluminum dome has a uniform thickness of 1.8 gm/cm^2 which bars protons < 39. MeV. Pulse height discriminator A1 at 0.72 MeV is able to count single protons, single electrons, and pileup electrons. Discriminator A2 at 2.6 MeV counts single protons only. The cross-section for counting mono-energetic protons with each of these discriminators is shown in Figure 1. Shielding over the back 2π steradians has been taken into account in computing the cross-section for high energy particles. For a power law spectrum of the form $J(E)dE = KE^{-n}\ dE$ discriminator A2 is approximated well by a rectangular passband between 40 and 110 MeV. The result of integrating these cross-sections over the above power law spectrum is plotted in Figure 2 as the effective geometric factor for computing $J(>40)$. With Figures 1 and 2 one can convert the counting rates given in this paper directly into flux for delta function and power law energy spectra. Other spectral forms require integration over the cross-sections given in Figure 1.

The other UCSD detector on Explorer 26 is a directional low energy particle counter, detector D. A cylindrical .25 x .25 cm plastic scintillator is coupled to a phototube and covered by a platinum cap containing an entrance hole 0.13 cm in diameter. An aperture of half angle 8^o defines the acceptance cone and gives the detector a directional

geometric factor of 8.38×10^{-4} cm^2 ster. An aluminum foil of 48 mg/cm^2 thickness and the discrimination levels, D1 at .28 MeV and D2 at .66 MeV, determine the particle types counted. D1 responds to electrons > .5 MeV and protons > 5 MeV, and D2 counts protons > 5 MeV and electrons with low efficiency. As an omnidirectional counter of penetrating radiation, detector D has a cross-section of about .055 cm^2 with shielding which averages more than 4.5 gm cm^{-2}.

For more particulars the reader is referred to McIlwain's (1966) description of an identical set of counters on Explorer 15.

III. ARRIVAL FROM THE SUN

Explorer 26 was able to monitor the arrival of solar protons during the events of February 5, 1965, March 24, 1966, and August 28, 1966. Figure 3 shows the March 24, 1966 event. The discriminator A2 counting rates, plotted as crosses, have been smoothed by averaging over intervals of variable length chosen to obtain good statistics without spoiling time resolution. The protons are attributed to an importance 3 flare, which started at 0225 UT and reached maximum brightness at 0240. The protons were first detected by Explorer 26 at 0303 ± 0003 UT and the counting rate peaked at 0325. Their pathlength in reaching the earth can be gauged from their propagation time and an estimate of their energy. The ratio of A1 to A2 counting rates at the peak is 1.6 : 1, which places the energy at 85 MeV if the particles are monoenergetic and sets an upper limit of 85 MeV on the average energy of any distributed spectrum. Inaccuracies in our knowledge of the detector gain and/or the cross-sections in Figure 1 could cause an error of ± 10% in this number. Then the time lapse from the start of the flare to the peak allows an interplanetary pathlength of only 3.3 AU.

Additional data on this event, obtained outside the magnetosphere by OGO-I, have been published by Kahler, Primbsch, and Anderson (1967). Their detector, which has a large geometric factor and high energy resolution, was unfortunately hampered by an anticoincidence failure which makes the geometric factor unknown. However, when their published data are adjusted to an equivalent energy range (channels 7 through 17 or roughly 40 - 140 MeV), an assumed omnidirectional geometric factor

of 1.5 cm^2 brings their fluxes within 50% of those measured by Explorer 26 during the arrival, peak, and decay phases of the event. As this geometric factor is compatible with their in-flight calibration of the OGO detector based on riometer absorption data, we conclude that the OGO-I and Explorer 26 intensities and onset times are in agreement.

The Vela data shown in Figure 3 were generously given to us by Dr. John Gosling of the Los Alamos Scientific Laboratory. The counting rates for Explorer 26 have been scaled by the ratio of geometric factors at 85 MeV. Although the Vela detectors were not designed primarily as proton counters, their responses are strikingly similar to Explorer 26. Simultaneity among all counters can be conservatively stated as better than 5 minutes, and the intensities seem to be as close as our knowledge of the geometric factors permits.

It is to be remembered that the Vela satellites are at 17 R_e, OGO-I was well outside the magnetophere, but Explorer 26 was inside on closed lines of force. At the position where Explorer 26 observed the peak flux of solar particles, the acceptance cone computed by classical Störmer theory for 85 MeV protons was only 1/10 of a sphere. Since Liouville's theorem disallows focusing, the detector should have been expected to see no more than one-tenth of the interplanetary flux. The problem of geomagnetic cutoffs will be discussed in a later section of this paper, but it is evident that the particles arriving from the sun are penetrating deep into the geomagnetic field, deeper than their Störmer cutoffs would allow.

The arrival of solar protons on February 5 is shown in Figure 4. Because of the low flux and the uncertainty in identifying galactic cosmic-ray background, the onset cannot be fixed precisely, but our best judgment is 1850 ± 0012 UT. The flare where the particles originated was seen from 1750 UT to 2024 with maximum brightness at 1810. On Mariner IV, in line with the earth 1.14 AU from the sun, three geiger tubes with a threshold of 55 MeV for omnidirectional protons recorded the onset of solar particles at 1835 ± 10 minutes (Krimigis and Van Allen, 1967). The reported arrival times are within only marginal agreement, but the discrepancy may be explainable. Explorer 26 was in such an orbital phase that it did not reach a very high L value, and the greatest intensity it measured fell short of that in interplanetary space. Thus it is probable that the geomagnetic cutoff affected its profile of the event, and may have contributed to the problematical earlier onset at Mariner.

During the solar proton event of July 7, 1966, Explorer 26 was in an unfavorable orbit so that neither the arrival nor the interplanetary intensity was monitored. Protons were counted, but the detector did not reach an L value above 5.2 and there is evidence that this was not above the 4π cutoff. Thus we can make the qualitative statement that protons did arrive at the earth, but we will present no quantitative observations.

The solar proton event of August 28, 1966 was initiated by an importance 3 flare that occurred at solar coordinates 21° N and 4° E. The flare started at 1523 UT and reached maximum at 1530. At 1629 particles arrived at Explorer 26, as seen in Figure 5. As the A1/A2 ratio soon after the arrival sets a limit of 95 MeV to the average energy in channel A2, the pathlength of these particles is no more than 3.8 AU. During five apogees when L was greater than 5.5 the average counting rate agreed tolerably with a predicted counting rate based on 1963 - 38C data (Bostrom, 1967) taken over the polar caps. (As it was necessary to extrapolate the 1963-38C spectrum from 25 to 40 MeV, this tolerance is loose, and estimated at a factor of two.) Therefore it is concluded that the geomagnetic cutoffs did not interfere with the measured arrival time and that the undiminished interplanetary flux was sampled several times afterwards.

The last event to be considered in this paper is that of September 2, 1966. The first detection of solar protons is shown in Figure 6. The particles arrived at the earth while Explorer 26 was inside the trapped radiation zone, but as Explorer moved out of the zone and approached apogee, the solar proton flux was still rising. At the beginning of the pass it is difficult to distinguish between the time dependence of the solar protons and the spatial dependence of the geomagnetic cutoffs. Measurements later in the event provide many samplings of the interplanetary intensity, the geomagnetic cutoffs, and the flux of solar particles which are in the geomagnetic field but not trapped. The following section of this paper will be devoted to these measurements.

For a concise list of data on these flares and the arrival of the solar particles at the earth the reader may refer to Table I. As the preceding discussion of these events has shown, solar particles arrived promptly at Explorer 26 if the satellite was in a favorable position. During most events Explorer 26 sampled the undiminished interplanetary intensity near apogee, and even obtained useful time profiles of the solar particle flux.

Table I

Solar Flares and Terrestrial Arrival of Solar Protons

Flares				Protons		
Date	Onset Time	Importance	Location	Arrival Time	Interplanetary Intensity Observed by Explorer 26	Cutoffs Observed by Explorer 26
2/5/65	1750	2	N8 W25	1850 ± 12	Not Observed	Not Observed
3/24/66	0225	2+	N20 W40	0303 ± 3	Figure 3	Not Observed
7/7/66	0020	2+	N34 W48	Not Observed	Not Observed	Not Observed
8/28/66	1523	2+	N22 E4	1629 ± 5	Figure 5	Not Observed
9/2/66	0542	3	N22 W58	Not Observed	Figures 6,8,10	Figures 6-9,11,13

IV. THE MOTION OF SOLAR PROTONS IN THE MAGNETOSPHERE

The Solar Proton Cutoffs

The September 1966 event was sufficiently intense for Explorer 26 to make meaningful observations of the solar protons deep within the magnetosphere. As expected, east-west asymmetry was exhibited at the lowest altitudes because of the strong density gradient of guiding centers where the solar particles ceased to penetrate. Here the cutoff is a function of detector look direction, with allowed and forbidden cones for the arrival of particles with any given energy. These cutoffs were well below their positions calculated according to Störmer for an infinite dipole field. However, Störmer's theory is still useful to describe the characteristics of their motion, and a modified Störmer theory gives a remarkably good fit to the data.

Ray (1963) derives the following formula for a particle's direction angle in an axially symmetric region of a magnetic field:

$$\cos\omega = \frac{2\gamma}{r \sin\theta} - A_\varphi \qquad (1)$$

The variables are defined as follows:

ω is the angle between the particle's velocity and west.

r, θ, φ are the radial distance, colatitude, and longitude.

A_φ is the azimuthal component of the magnetic vector potential.

γ is an initial condition with units of length. For a cosmic ray in a field that vanishes at infinity, 2γ is the impact parameter of the particle's initial trajectory.

Length is expressed in energy-dependent Störmer units given by

$$C_{st} = \sqrt{\frac{eM}{mvc}}$$

or the square root of the ratio between the earth's dipole moment and the particle's rigidity. At the low L values where the solar particles coexist with trapped electrons, it is assured that the lines of force

have a dipole-like mirror geometry and form closed shells axially about the earth. Thus, in this region a dipole term is a reasonable first approximation to $A\varphi$, and

$$\cos\omega(\gamma) = \frac{2\gamma}{r \sin\theta} - \frac{\sin\theta}{r^2} \tag{2}$$

For a given energy particle at a given point in space equation 2 determines the relation $\omega(\gamma)$ between the particle's direction angle and the integration constant γ. If there is any restriction on the possible values of γ, there may be a restriction on the allowed values of ω. For instance, in the classical Störmer problem where the field is dipolar out to infinity, there is a maximum value of γ for which cosmic ray (unbounded) trajectories can penetrate below a gate point one C_{st} from the origin. In Ray's notation this is given by

$$\gamma \leq 1 \tag{3}$$

The allowed values of ω determined by such a limit on γ form a cone which has its axis on the east-west vector. As the observation point moves inward, the allowed cone shrinks from a full sphere above

$$r_+ = \frac{\gamma_{max} - \sqrt{\gamma_{max}^2 - \sin^3\theta}}{\sin\theta} \tag{4}$$

to only the eastbound hemisphere at

$$r_c = \frac{\sin^2\theta}{2\gamma_{max}} \tag{5}$$

and finally to the last eastbound ray at

$$r_- = \frac{-\gamma_{max} + \sqrt{\gamma_{max}^2 + \sin^3\theta}}{\sin\theta} \tag{6}$$

The additional consideration of earth-shadow cones is clearly unnecessary because of the high altitude of the Explorer 26 orbital observations.

Figure 7 illustrates a roll modulation of the detector counting rate caused by this east-west asymmetry during a pass in which the satellite remained below r_+. Because the orientation of the spin vector is unknown, the amplitude and phase of the modulation cannot be tested theoretically. However, the spin-averaged counting rate is the true omnidirectional rate, and this can be related to the interplanetary rate as will be shown later in this section.

Above r_+ the interplanetary flux arrives unattenuated. This feature appears as an isotropic plateau like those seen in Figures 8 and 9 which are typical of the Explorer 26 data from this event. The roll modulation appears in these figures as an asymmetric domain where the intensity changes rapidly at the beginning and end of the plateau. These two features, a domain of east-west asymmetry and an isotropic plateau, appear on pass after pass during this event until the counting rate becomes so small that it is impossible to distinguish them. The spatial occurrence of these features is represented schematically in Figure 10 which shows the satellite trajectory for six passes plotted on a topographical flux map of B, L space. Intervals of roll modulation are depicted by heavy dashed lines, and the plateau by a solid black line. It is evident that the plateau extends outward indefinitely and has a flat profile, which is expected of the unattenuated solar flux.

The plateau edge advances progressively inward from the first to the last pass shown. This interval is the buildup period of a geomagnetic

storm associated with the proton-emitting flare, and the advance is caused by distortion of the magnetosphere. The dependence of the solar proton cutoffs on geomagnetic storm parameters is an interesting topic that will be discussed separately in a later section of this paper.

There is a time variation in the plateau flux, consisting of an exponential decay with a time constant of about 8 2/3 hours, visible in Figure 8. The profiles of 13 passes are shown in Figure 11 , with schematic representation of isotropy and roll modulation. The same decay is seen from apogee to apogee and persists for several days with the same time constant. This time dependence is determined by the interplanetary propagation of the particles, which is the subject of section V of the paper.

The intensity of the equatorial plateau can be checked against the interplanetary flux by comparing measurements made by spacecraft inside and outside the magnetosphere. For the March 1966 event such a comparison was possible with OGO-I and Vela 2A and 2B, with the results shown in Figure 3 and discussed previously in this paper. For September 1966 data are available from two low altitude, polar orbiting spacecraft, 1963-38C and 1966-70A. (Bostrom 1967; Paulikas, Blake, and Freden, 1968) There is some doubt whether the polar cap field lines connect directly to the interplanetary field or form an extended tail. However, this matters only for lower energy protons, since above 40 MeV the polar plateau is directly accessible from space. Data from the two polar orbiting spacecraft were taken in 3 integral energy ranges from 2.2 to 25 MeV (1963-38C) and in 8 differential ranges from 1.1 to 130 MeV (1966-70A). To be compared with Explorer 26

the measured polar cap spectra were interpolated or extrapolated over the energy range of detector A2, background corrections made and geometric factors adjusted, assuming isotropy, to obtain the counting rate that would have been obtained by Explorer 26 over the pole. These data are displayed in Figure 11, and it is clear that not only the intensity but also the time profile of the event is in agreement.

Now it is appropriate to make the observation that in the asymmetric domain the fraction of a sphere subtended by the allowed cone determines the true omnidirectional rate in relation to the interplanetary counting rate. Because the spin-average counting rate is the true omnidirectional rate, we can write

$$\overline{CR} = J_p \, G \, \frac{\Omega (\gamma_{max})}{4 \pi} \tag{7}$$

where $\overline{CR}$ is the spin averaged counting rate

J_p is the omnidirectional interplanetary flux (assumed isotropic) in cm^{-2} sec^{-1}

G is the omnidirectional geometric factor in cm^2

and

$$\Omega (\gamma) = 2 \pi (1 + \cos \omega (\gamma)) \tag{8}$$

Where the field is axially symmetric (1), (7), and (8) relate $\overline{CR}$ to J_p, and, if the dipole assumption is good,

$$\overline{CR} = \tfrac{1}{2} J_p G \left(1 + \frac{2 \gamma_{max}}{r \sin \theta} - \frac{\sin \theta}{r^2} \right) \tag{9}$$

This equation relates the interplanetary counting rate to the spin-averaged counting rate at a given position r, θ. Because it is written in Störmer length units, it applies to a single energy. However, as the Störmer length is a mild function of energy ($C_{st} \alpha E^{-\frac{1}{4}}$ for non-relativistic particles), a single value of C_{st} contains wide latitude. Therefore we will use the upper limit to the average energy provided by the A1 : A2 ratio as we did in section III. Throughout the event this ratio is close to 3 : 2, which determines an energy of 80 MeV and sets C_{st} at 12.2 earth radii.

The other quantities for equation (9) can be read from the graphs. The interplanetary flux is measured on the plateau of each pass, and an exponential term allows for the time variation:

$$J_p = J_o \exp (- (t - t_o)/ \tau) \qquad (10)$$

γ_{max} is fixed, for a dipole field, by (3). However, as we have already observed, pure Stormer theory does not work. Therefore let us treat γ_{max} as an empirical quantity. It can be evaluated very easily. To be consistent with the earthbound convention of measuring vertical cutoffs, we define the cutoff at satellite altitudes as the limit for vertical arrival of particles of a given rigidity. This is where $\cos\omega = 0$, the allowed cone equals one hemisphere, and $\overline{CR}$ falls to one-half its interplanetary value. Equations 5 and 9 give the cutoff location for a dipole field. It is a line of force, given by

$$L_c = \frac{1}{2 \gamma_{max}} \qquad (11)$$

Ray (1963) has shown that for a more general axially symmetric field the vertical cutoff rigidity is still constant along a line of force. Therefore we denote by L_c the L value where $\overline{CR}$ falls to half its interplanetary value and use (11) to evaluate γ_{max}. From graphs such as Figures 8 and 9, it is easy to find values for J_o, t_o, and τ in (10) and to read off, for the outbound and inbound legs separately, values for L_c in (11). Equation 9 can then be used to give $\overline{CR}$ as a function of r and θ, and this can be compared with the experimental profile of the plateau edges.

This procedure has been carried out for the several passes during this storm. The dashed line in Figure 8 is the result for pass number 5. Agreement with the observed counting rate profile is good. Figure 6 shows a more difficult situation at the onset of the event where the satellite did not measure the interplanetary flux and where the intensity was increasing at an unknown rate. By trial and error adjustment of the intensity, time constant, and one cutoff, a satisfactory fit was obtained, as shown by the dashed line. Pass 3 shares with pass 1 the difficulty that the interplanetary flux was not measured, although the decay time can be safely assumed the same as in the neighboring passes. Adjustment of the intensity and one cutoff gives the fit shown in Figure 7. This is the worst fit of the series, and shows need of a different γ_{max} for the outgoing and incoming legs of the pass. Pass 2, Figure 9, is very satisfactory, and the fit becomes an interpretative aid by giving evidence that the satellite grazed r_+ for a long time on the way out. In all but the two passes mentioned the parameters of the interplanetary flux are measured separately from

the cutoffs. Thus the position and width of the cutoff profile are determined by only one parameter, γ_{max}, and for a variety of cases this gives a good fit to the data. This success suggests that in high altitude surveys the word cutoff is most meaningfully applied to that point where the omnidirectional intensity falls to half the plateau value, and that this measurement is interpretable in terms of a modified Störmer theory.

Values of the fitting parameters used for eight passes during this event are listed in Table II. In some cases an improvement in γ_{max} was possible using a best-fit criterion rather than reading L_c from the graph. The table shows best-fit values. The departure from Störmer theory is evident, as in every instance γ_{max} is greater than unity. In this regard it should be noted that the use of the maximum average energy allowed by the A1 : A2 ratio gives a minimum value for C_{st} and thus a minimum value for γ_{max}. A more realistic C_{st} would be slightly larger, and would increase γ_{max} and slightly lower the quality of the fits in Figures 6 - 9.

Table II

Modified Störmer Cutoff Analysis

Pass	t_o (days)	J_o (c/s)	t (day)	γ_{max} Outbound (C_{st})	* Inbound (C_{st})
1	245.333	7.0	-.0715	1.12	1.12
2	245.75	155.	.36	1.15	1.33
3	246.0	90.	.36	1.15	1.15
4	246.333	37.	.36	-	-
5	246.5	16.	.36	1.55	1.49
6	247.0	4.5	.36	1.53	1.58
7	247.25	1.52	.36	1.63	1.565
8	247.5	1.2	.36	1.63	1.4
9	247.875	0.65	.36	1.245	1.285

* C_{st} was taken as 12.2 R_E for all passes.

The modified Störmer theory given here could be refined, but too many unknowns creep in that are not resolvable by the present experiment. For instance a distributed energy spectrum can be considered by using in equation 9 a suitably averaged C_{st}. However this generalization introduces a need to know the energy dependence of γ_{max}. An experiment with multiple energy windows is desirable to resolve this unknown. As another refinement one could consider a γ-dependent transmission coefficient at the gate, as suggested by Ray (1964). Again, more measurements are needed to resolve this dependence. An important refinement would be to extend the theoretical formulation to an asymmetrical magnetosphere. Efforts in this direction undertaken by Friedland (1967) show a discouraging complexity.

Separation of Trapped and Untrapped Particles

The spatial proximity of the untrapped solar protons to the trapped electrons and protons may shed light on the physical conditions for adiabatic trapping. If there exists a geometrical boundary which sets the observed limits of trapped and untrapped motion, it should be the minimum distance at which protons directed due west can remain untrapped. This distance, given by equation 4, is r_+, the edge of the proton plateau. It may or may not be that r_+ is the outer trapping limit for electrons. We have seen in Figures 5 through 9 that the electron fluxes decrease approaching the proton plateau and fall to zero shortly past the edge. As it is most unlikely that we have mistaken the plateau edge, the electrons detected past this position challenge the geometric boundary model. If they mirror at the same

position as the protons, the distinction between adiabatic and non-adiabatic motion must be determined by the difference in their rigidities, not by the field geometry. On the other hand, if they mirror at higher latitudes than the protons, they may be attributed to shell-splitting. As shown by Roederer (1967) there is a zone around the equator on the night side of the earth where particles with small pitch angles can be permanently trapped but those with large pitch angles are psuedo-trapped. This is, they cannot complete a drift longitudinally around the earth without being lost. Thus trapped and untrapped particles can appear on the same line of force, but with different pitch angles. Because the electron pitch angles are not measured, this explanation cannot be checked and the possibility of a geometrically determined trapping boundary remains open.

Direct entrapment of solar protons has been thought of as a possible source for the high-energy radiation belts. Therefore, it is of interest to examine the separation between trapped and untrapped particles of the same rigidity to see whether any merging occurs. In Figures 4 through 9 and in all other passes the two zones of energetic protons are entirely separate; between them is a barrier where no protons are found. The barrier counting rate of .1 to .2 shown in Figures 5 through 9 represents an upper limit, as it is determined by the reciprocal of the interval between successive counts, and the satellite passes from one zone to the other in a time smaller than the average interval between background counts. Therefore there is no support for direct entrapment, although the mechanism is too problematical for a strong case to be established against it.

V. INTERPLANETARY DIFFUSION OF SOLAR PROTONS

It has been established that the plateau represents the interplanetary value of the proton flux. Therefore our data are relevant to yet another topic concerning solar protons: their propagation in interplanetary space. Because of the nature of the detector, directional or spectral discrimination is impossible, but good intensity-time profiles were obtained during the events of March and September 1966. (See Figures 3 and 11.)

Models of interplanetary propagation in which the protons undergo a random walk can be represented by diffusion equations where the solutions predict the time dependence of the intensity at earth. Let us consider the models of Axford (1965), and of Parker (1963) as developed by Krimigis (1965). In the latter model the dimensionality of space is represented in general form by an index α, and an isotropic diffusion equation is written in which the diffusion coefficient varies as x^{β}, where x is the distance to the sun. For an initial condition consisting of impulsive injection at the origin, the solution predicts that

$$\ln \quad (J\ t^{n}) = C_1 + C_2\ (1/t) \tag{12}$$

where

$$n = \frac{\alpha + 1}{2 - \beta}$$

In testing this model against experimental data, various values of n are tried with the purpose of finding one that orders the data in the straight line given by (12).

The position of the sun on the solar disc does not enter into this model, although observationally it is known to be important. Axford

provides for such a position dependence by assuming that particles which reach the earth must first diffuse in two dimensional space over the face of the sun from the flare to the tube of force that encloses the earth. Their subsequent diffusion to the earth follows the same equation adopted by Krimigis, with x^{α} being defined by Axford as the variation of the cross section of the tube of force. Because of this similarity the solutions for the two models approach the same form for large t.

Position dependence also results if one uses an anisotropic diffusion equation. Fibich and Abraham (1965) discuss such a model and derive a result for large t which follows (12) with n = 3/2. Burlaga (1967) has also developed an anisotropic model with the additional feature of an absorbing boundary 1 or 2 AU beyond earth. During the rise Burlaga looks for n = 5/2 in (12), followed by an exponential decay which is imposed by the boundary.

Evidently a relation in the form of (12) and the trial method used by Krimigis is a sort of universal test for many diffusion models. The new data for the March and September storms have been plotted by this technique with negative or indecisive results. Because of their unsatisfactory nature these graphs are not shown, but some discussion is appropriate.

The sharp peak in the March event's profile cannot be straightened out. This is true also for the Vela data and agrees with Kahler, Primbisch, and Anderson's OGO-I analysis. During the decay phase alone,

$n = 3$ in equation 12 is not out of the question, but during the onset no choice of n yields a good result, even when the zero time is varied. It must be acknowledged, though, that the onset of an event is more difficult to test than any other phase, because the low counting rates cause statistical errors, velocity dispersion causes bad energy identification, and the errors of assuming a delta function injection and identifying the zero time are more critical. The flare which triggered the March event occurred at 42° W solar longitude, evidently at the foot of that tube of force that contained the earth. The narrowness of the peak is out of keeping with diffusive behavior and the conclusion of Kahler, Primbsch and Anderson, that the particles underwent too few scatters to obey a diffusion law, may be essentially correct.

The September event was of longer duration and more nearly resembles a diffusion model. The best fit to the data comes between $n = 4$ and 4.5, with no systematic deviation from a straight line. There are, however, many short term departures far outside statistical error. For large t equation 12 approximates a power law decay with exponent n, but as can be seen in Figure 11, there are irregularities in the decay curve which deviate from such a law. Among possible explanations for these irregularities are filamentary structure in interplanetary space, particle storage, emission of new particles, and time variations of the propagation conditions. Because two new flares occurred on September 4 and 5, the last two hypotheses deserve special consideration. The poor time correlation between the new flares and flux increases causes us to reject the possibility of new particle emissions. However, each

of the new flares, as well as the original flare, triggered a magnetic storm and a Forbush decrease 1 1/2 to 3 days later at the earth. Here is evidence for variation in interplanetary conditions, and irregularities in the data might be explained by a boundary's sweeping past the earth with each storm front and establishing a new interplanetary order.

VI. THE CUTOFF ALTITUDE DURING A MAGNETIC STORM

In section IV we pointed out that the solar proton cutoffs decreased during the geomagnetic storm of September 3 - 4, 1966. Table III lists the cutoffs read from the data without benefit of a best fit to the modified Störmer theory. Included are information regarding the position of the satellite and the values of two geomagnetic parameters at the time of the measurements. In this section and in the appendix we will investigate the correlation of the cutoff altitude with magnetic storm parameters and consider their cause and effect relationships. Specifically, we shall prove that a mechanism stronger than the ring current causes the cutoffs to be lowered.

Figure 12 shows a plot of the data vs. time. D_{st} is a measure of the geomagnetic ring current, and has been computed two ways. A ground-based measurement was obtained by averaging the departures from the normal horizontal field components at San Juan and Honolulu. The other, satellite-based determination was made by measuring the reduction of the trapped proton flux caused by betatron deceleration and computing the ring current required to produce this effect after the fashion of McIlwain (1966).

Additional ground-based measurements of the ring current are shown in Figure 13, where the horizontal component is shown for five stations equally spaced about the equator. In this figure we can see the degree of asymmetry of the ring current as well as the presence of bay activity, often near local midnight.

TABLE III

TABLE OF SOLAR PROTON CUTOFFS@ OBSERVED BY EXPLORER 26 AFTER THE SEPTEMBER 2, 1966 FLARE

Date	Time	Local Time	B/B_o*	L*	D_{st}**	K_p
9/2/66	0954	2218	2.045	5.2± .1	-14	2-
9/2/66	1425	1925	2.018	5.3± .05	- 7	3-
9/2/66	1804	2328	2.962	4.65± .05	+ 7	4_o
9/2/66	2344	2018	1.0775	5.1± .15	- 4	3_o
9/2/66	2351	2125	1.129	5.1± .15	- 4	3_o
9/3/66	1142	1808	1.654	3.9± .1	-42	6-
9/3/66	1631	0002	3.067	4.1± .1	-58	6_o
9/3/66	1909	1819	1.029	3.75± .1	-70	7+
9/3/66	2345	2340	1.395	3.75± .15	-154	9-
9/4/66	0236	1822	1.020	3.7± .1	-198	9-
9/4/66	0654	2311	1.196	3.9± .05	-184	7+
9/4/66	0947	1800	1.652	3.75± .2	-133	6_o
9/4/66	1434	2345	3.011	4.35± .1	-99	6-
9/4/66	1812	1924	1.361	4.9± .2	-105	3+
9/4/66	2122	2242	1.747	4.75± .2	-90	3_o

* B, L computed from internal fields only.

** D_{st} obtained by averaging the horizontal component at San Juan and Honolulu, after subtracting the quiet day averages from August and September. D_{st} is given in γ ($1\gamma = 10^{-5}$ gauss)

@ Cutoffs measured as the L value where the east-west average solar proton flux falls to half the plateau value.

The cutoff L value is plotted against each of the two geomagnetic parameters in Figure 14. The thin trace on the left hand plot follows the time sequence of the points, ordered counterclockwise. Because outbound crossings occur in the local evening near the equator, whereas inbound crossings occur at higher latitudes near local midnight, the crossings have different symbols. It is uncertain whether or not this distinction helps to order the data.

This figure shows the correlation between the cutoff and each geomagnetic parameter directly. K_p was used for this study because of its long-standing, universal application to geomagnetic disturbances. The ring current index was chosen because it has played a prominent part in the theories proposed to explain the sub-Störmer penetration of cosmic rays. We see a better correlation with K_p, D_{st} lagging in phase behind the cutoff. However, our strongest argument against a ring current cause for the lowered cutoffs is based on the polarity of the change, not just on its phase. Cosmic rays which come no closer to the earth than 3 1/2 to 5 earth radii remain outside the region where the ring current's effect would lower their cutoffs. These particles see the ring current from the outside, where the first and main term in an expansion of the disturbance field is a dipole of the same polarity as the earth's dipole. Strengthening the earth's dipole moment should raise the cutoff, because it increases the Stormer unit, and thus the length scale of the resulting cutoffs.

This argument is not precise, of course, although it should render the result plausible. An airtight argument requires considerably more

detail, and since our conclusion is that a ring current is not the principal mechanism, this argument is relegated to the appendix. There a Störmer-like calculation is done for the equatorial plane, and it is shown that any symmetrical model of the ring current, the magnetospheric boundary current, or the ring and boundary currents combined tends to raise the equatorial cutoff altitude. The observations of course do not disprove that a ring current exists or that it tends to change the cutoffs as calculated. They merely prove that there is another mechanism which acts in the other direction at the equator and is more effective there. It is natural to suppose that the other mechanism is more effective also at the earth's surface where the ring current does operate in the right direction.

A word of justification may be desired regarding the apparent paradox that a symmetrical ring current acts to raise the cutoff at the equator and to lower it at the earth's surface. If we use the result of Sauer and Ray (1963) that the cutoff rigidity is constant along a line of force, the paradox demands that there is a storm-time line of force which has its foot at a lower latitude and crosses the equator at a higher altitude than a quiet-time line of force. This is entirely reasonable. A ring current inflates the magnetosphere and stretches the lines of force outward at the equator, so that the above demand can be met.

With the ring and boundary current discounted as the primary cause of the storm-time cutoff depression, that agent which seems most likely to produce such an effect is the geomagnetic tail. Indeed, Reid and

Sauer (1967) and Gall, Jiménez, and Camacho (1967) have recently proposed that this is the cause. Although our data cannot prove this hypothesis, they may at least provide a modest test. By trajectory integration, Gall et al. showed that at the earth's surface the cutoff rigidity at a given latitude is reduced by an increase in the tail field strength. It also follows that the cutoff latitude for a given rigidity is so reduced. If we use the experimental results of Behannon and Ness (1966) that, statistically, the tail field strength correlates positively with K_p, it follows that cutoff latitudes should correlate negatively with K_p. This result has been shown by Lin and Van Allen (1964), although at the time they attributed it to the ring current. The test for a similar explanation of the correlation between equatorial cutoff and K_p is to demonstrate that a strengthened tail reduces the equatorial cutoff rigidity and altitude. This result is to be expected from trajectory integrations in the fashion of Gall et al., since their magnetospheric model contained no ring current, and therefore undistorted connection is expected from the earth's surface to the equator.

VII. DISCUSSION AND CONCLUSIONS

The conclusion stated in section VI that an asymmetric field is needed to lower cosmic ray cutoffs establishes a new perspective with which to review our discussion in section IV concerning the motion of solar protons in the magnetosphere. It may seem that the asymmetry demanded by section VI and the appendix threatens section IV's modified Störmer theory, based as it is on axial symmetry. The explanation of this paradox is that section IV used axial symmetry only in the vicinity of the cutoff altitude, r_c, giving up the Störmer condition on γ_{max}. In the appendix the demand for asymmetry was based on the contrary effects of axially symmetric perturbations on γ_{max}. Since γ_{max} is established by conditions at the gate altitude, r_g, asymmetry is demanded no lower than this. Our discussion is self consistent if the field loses its symmetry somewhere between r_c and r_g. Then the appendix actually complements section IV, as it clarifies the meaning of γ_{max} and justifies the departure from Störmer's value.

Notwithstanding the possibility of a self-consistent discussion, the experimental data still belie the assumption of axial symmetry used in the modified Störmer model. In tables II and III and Figures 12 and 14 the difference between outbound and inbound cutoffs is most likely to be a local time effect. Furthermore, other measurements have clearly established that solar proton cutoffs exhibit local time asymmetry (Paulikas et al, 1968; Stone, 1964). Therefore the modified Störmer model must be regarded as a stage of approximation. It is good enough to describe directional cutoffs, acceptance cones, and r, θ profiles. A parameteric study of γ_{max} should yield valuable insights. However,

refinements are desired as suggested in section IV, and particularly a local time dependence is needed.

This area, which is a deficiency of the Störmer theory, is the strong point of the proposal by Reid and Sauer. In a model which is carried out in the noon and midnight meridians, they propose that the limits of trapped and untrapped motion occur at a geometrical boundary. Setting the position and height of this boundary on the night side determines a cosmic ray cutoff, and quasi-adiabatic drift maps this cutoff onto the day side. Satisfactory local time effects can be thus obtained. Because of the arbitrary handling of the nightside boundary, this model is too ad hoc to be physically satisfying, but it does provide an interesting hypothesis and an appealing rationale for the influence of the geomagnetic tail.

The most rigorous proof for the tail's effect on geomagnetic cutoffs is offered by Gall et al (1967). Using the Mead-Williams magnetosphere, which is the most complete model available, they have done trajectory integrations for particles arriving at the earth's surface. Their results include both a lowering of the cutoffs with increasing tail field strength and a local time variation. The penalty for such rigor, of course, is that the computer integration tends to mask systematic effects and fails to simplify the results.

In conclusion, we believe that the geomagnetic tail is the primary agent in lowering solar cosmic ray cutoffs. The observations made by Explorer 26 and reported in this paper prove that the ring current has a secondary influence, and the models and calculations discussed here point to the tail as the most effective agent.

Its low inclination, high eccentricity orbit also enabled Explorer 26 to take prolonged samples of the interplanetary intensity during apogees. The initial arrival of particles was recorded February 5, 1965, March 24, 1966, and August 28, 1966, and useful time-intensity profiles were obtained March 24, 1966 and September 2 - 6, 1966. These two cases probe the limitations of interplanetary diffusion models. In the former case it is thought that the particles reached the earth before collisions had randomized their velocities sufficiently to establish a diffusion regime. In the latter case departures from a simple diffusion time profile seem to be associated with interplanetary disturbances which changed the order of the magnetic field.

During the September event useful measurements were also obtained of solar proton intensities and anisotropies in the magnetosphere. It is shown that a modified Störmer theory is a satisfactory model for predicting the size of the acceptance cone and thus the cutoff profile of the omnidirectional counting rate.

Figure Captions

Figure 1 The effective cross-section of detector A versus energy. This is the geometric factor for a delta function energy spectrum.

Figure 2 The geometric factor of detector A for a power law energy spectrum.

Figure 3 The solar proton event of March 24, 1966 as seen by Explorer 26 and Vela. The count rate scale for Explorer 26 has been adjusted to match that of Vela for 85 MeV protons. Local time at Explorer is near midnight.

Figure 4 The arrival of the February 5, 1965 solar protons. The position of the satellite in B, L space is given by the L scale on the top of the figure and the B/B_{EQ} trace versus time. Local time is 16 hours to 19 hours.

Figure 5 The onset of the August 28, 1966 solar proton event. B and L for the satellite are given by the L scale at the top of the figure and the B/B_{EQ} trace versus time. Trapped electrons are shown on the lines of force with the untrapped protons.

Figure 6 The solar proton event of September 2, 1966, pass one. The orbit of Explorer 26 during this pass is shown in Figure 10. This is the first pass after the flare, and the interplanetary intensity is increasing with time.

Figure 7 The solar proton event of September 2, 1966, pass three. The orbit of Explorer 26 during this pass is shown in Figure 10. Strong east-west effect demonstrates the directional dependence of particle cutoffs. The modulation frequency is an alias of the actual spin rate.

Figure Captions (Continued)

Figure 8 The solar proton event of September 2, 1966, pass five. The orbit of Explorer 26 during this pass is shown in Figure 10. The plateau covers a wide range of B and L, with east-west modulation at the borders. The slope of the plateau matches the decay rate measured from pass to pass.

Figure 9 The solar proton event of September 2, 1966, pass two. The orbit of Explorer 26 during this event is shown in Figure 10.

Figure 10 The orbit of Explorer 26 during the solar proton event of September 2, 1966. Six orbits outside the boundaries of the trapped radiation are shown in B, L space, where B is normalized to the equator. A thin line represents the track of the satellite where data were taken. The dashed line indicates east-west asymmetry or strong spatial gradients of the solar particles. The solid line represents periods where the counting rate has reached a nearly constant plateau. Maximum L occurs at 2100 local time and the northbound equator crossing (ascending node) is at 0420 local time.

Figure 11 The time history of the September 2, 1966 solar proton flux. Explorer 26 apogee counting rates are compared with polar cap data obtained by Bostrom with 1963-38C and Paulikas with 1966-70A. The measured polar cap fluxes were extrapolated over the energy range of detector A2, and appropriate geometric and background corrections made to compare with Explorer 26. The ends of the error bars represent exponential versus power law extrapolation, and the position of the dot represents the author's judgment as to which is better.

Figure Captions (Continued)

Figure 12 The time sequence of cutoffs measured by Explorer 26 and other geomagnetic data. The cutoffs were measured as the L value where the east-west average solar proton flux fell to half the plateau value. Ground-based D_{st} was obtained by averaging the horizontal component at San Juan and Honolulu, after subtracting the quiet day averages from August and September. D_{st} was also determined from the satellite by measuring the adiabatic betatron deceleration of the trapped protons and computing the uniform ring current field required to produce this effect. Open circles denote outbound crossings and closed circles, inbound crossings.

Figure 13 Local time survey of the ring current of September 3 - 4, 1966. Hourly scalings of the horizontal component are shown for five near-equatorial ground stations. Local midnight is denoted by an M.

Figure 14 Relation between the equatorial proton cutoffs and two geomagnetic parameters for the event of September 2, 1966. Open and closed circles denote outbound and inbound crossings, respectively. The time sequence is shown by the light trace on the left-hand curve.

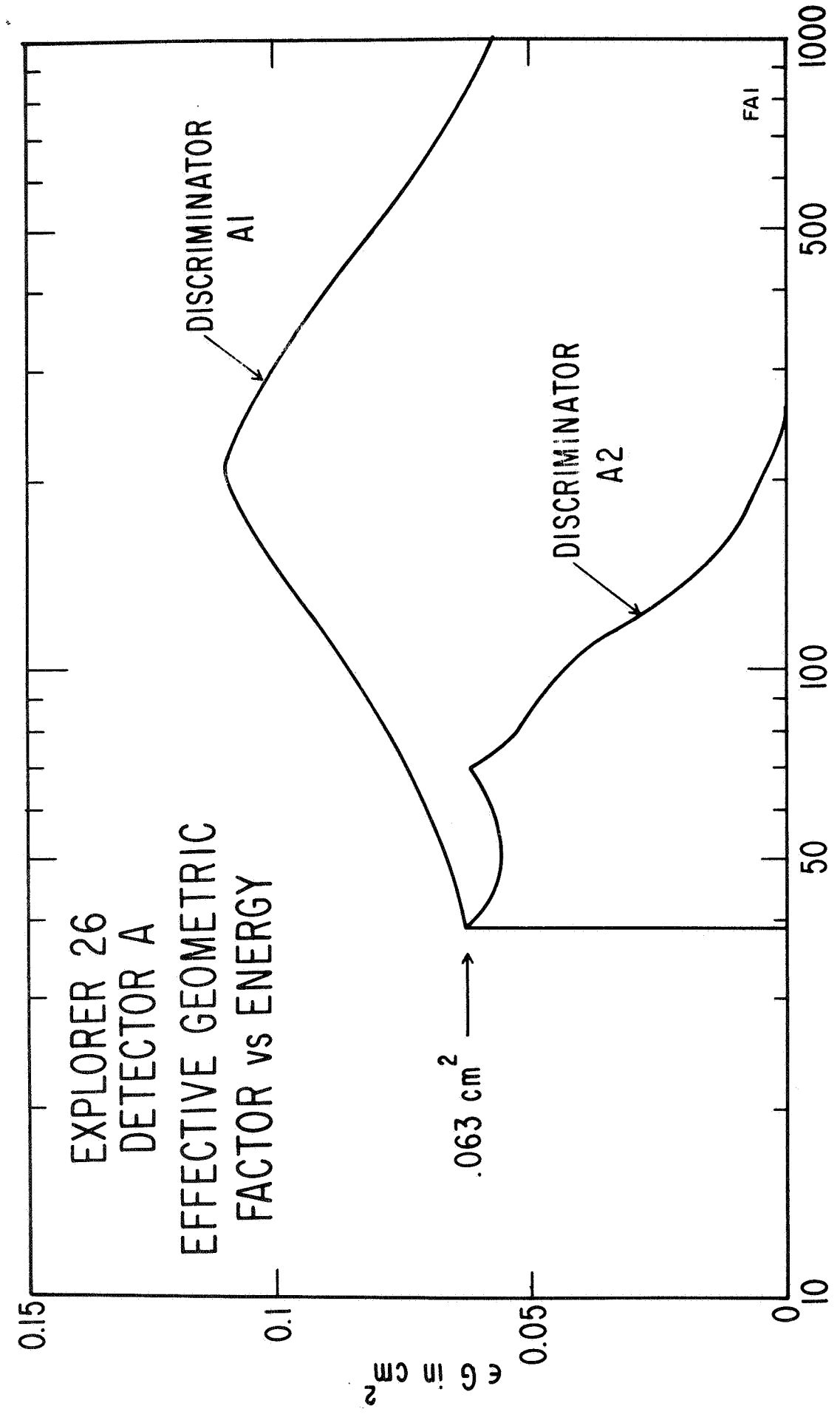
EXPLORER 26
DETECTOR A
EFFECTIVE GEOMETRIC
FACTOR vs ENERGY
DISCRIMINATOR
A1
DISCRIMINATOR
A2
.063 cm²
FA1
PROTON ENERGY, MeV
ε G in cm²
0.15
0.1
0.05
0
10
50
100
500
1000

Figure 1

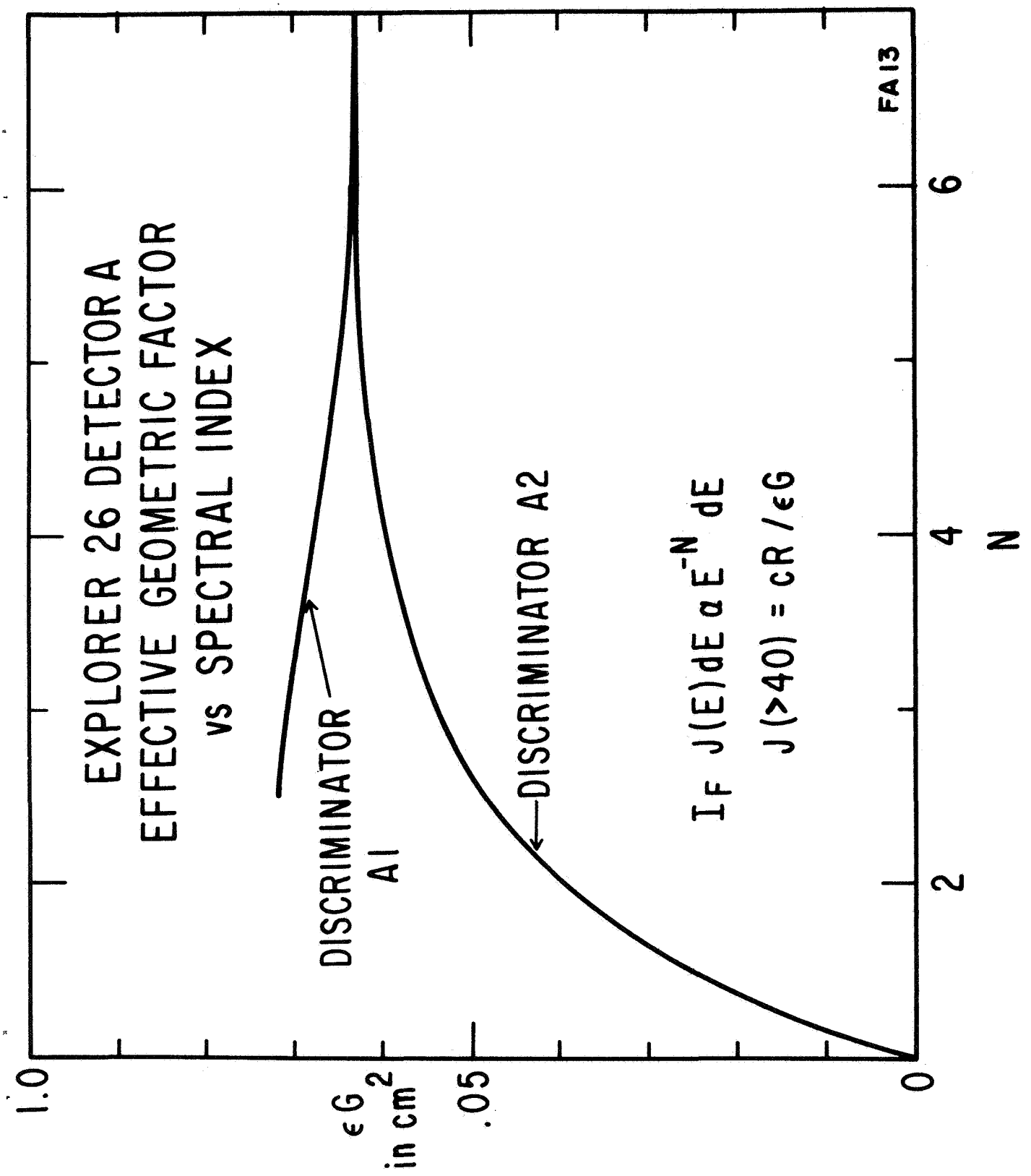
EXPLORER 26 DETECTOR A
EFFECTIVE GEOMETRIC FACTOR
vs SPECTRAL INDEX
DISCRIMINATOR
A1
DISCRIMINATOR A2
$I_F \int J(E)dE \propto E^{-N} dE$
$J(>40) = cR/\epsilon G$
ϵG_2
in cm^2
1.0
.05
0
2
4
6
N
FA13

Figure 2

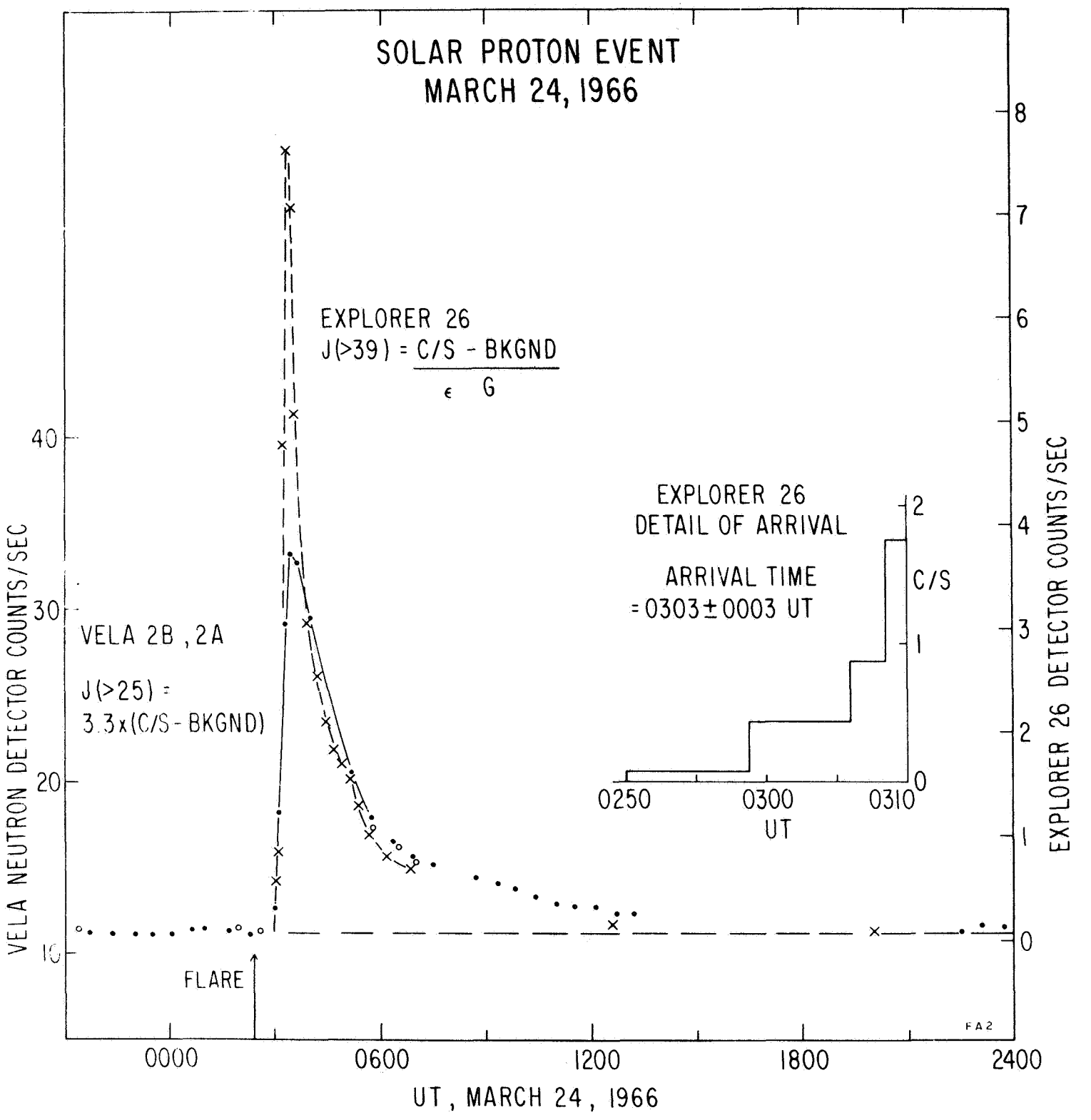
SOLAR PROTON EVENT
MARCH 24, 1966
EXPLORER 26
J(>39) = C/S - BKGND / ε G
VELA 2B, 2A
J(>25) =
3.3x(C/S - BKGND)
EXPLORER 26
DETAIL OF ARRIVAL
ARRIVAL TIME
= 0303 ± 0003 UT
C/S
0250
0300
0310
UT
FLARE
VELA NEUTRON DETECTOR COUNTS/SEC
EXPLORER 26 DETECTOR COUNTS/SEC
0000
0600
1200
1800
2400
UT, MARCH 24, 1966
FA2

Figure 3

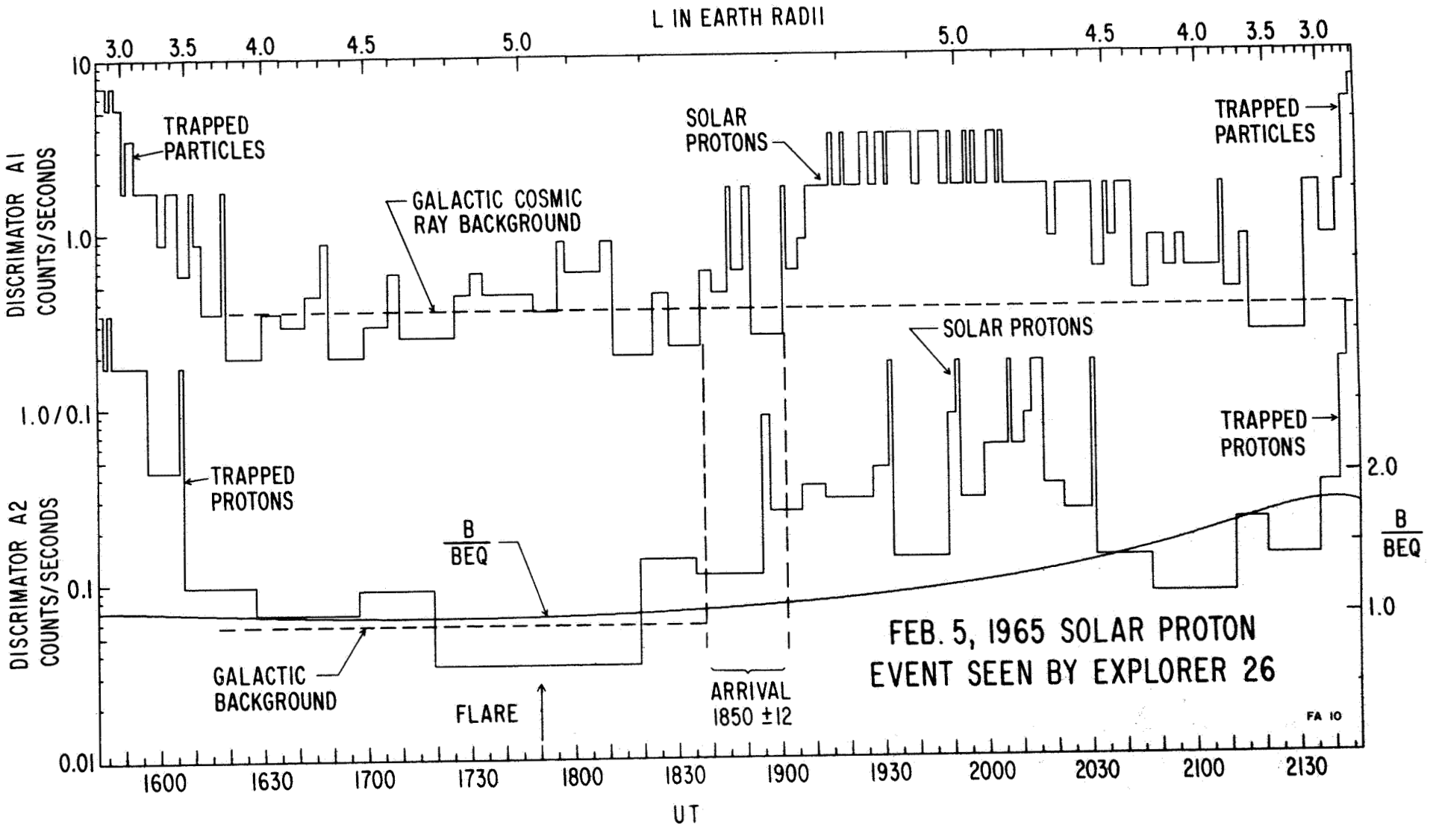
L IN EARTH RADII
3.0
3.5
4.0
4.5
5.0
5.0
4.5
4.0
3.5
3.0
10
1.0
1.0/0.1
0.1
0.01
DISCRIMATOR A1
COUNTS/SECONDS
DISCRIMATOR A2
COUNTS/SECONDS
TRAPPED
PARTICLES
GALACTIC COSMIC
RAY BACKGROUND
SOLAR
PROTONS
TRAPPED
PARTICLES
SOLAR PROTONS
TRAPPED
PROTONS
TRAPPED
PROTONS
B
BEQ
2.0
1.0
B
BEQ
GALACTIC
BACKGROUND
FLARE
ARRIVAL
1850 ±12
FEB. 5, 1965 SOLAR PROTON
EVENT SEEN BY EXPLORER 26
FA 10
1600
1630
1700
1730
1800
1830
1900
1930
2000
2030
2100
2130
UT

Figure 4

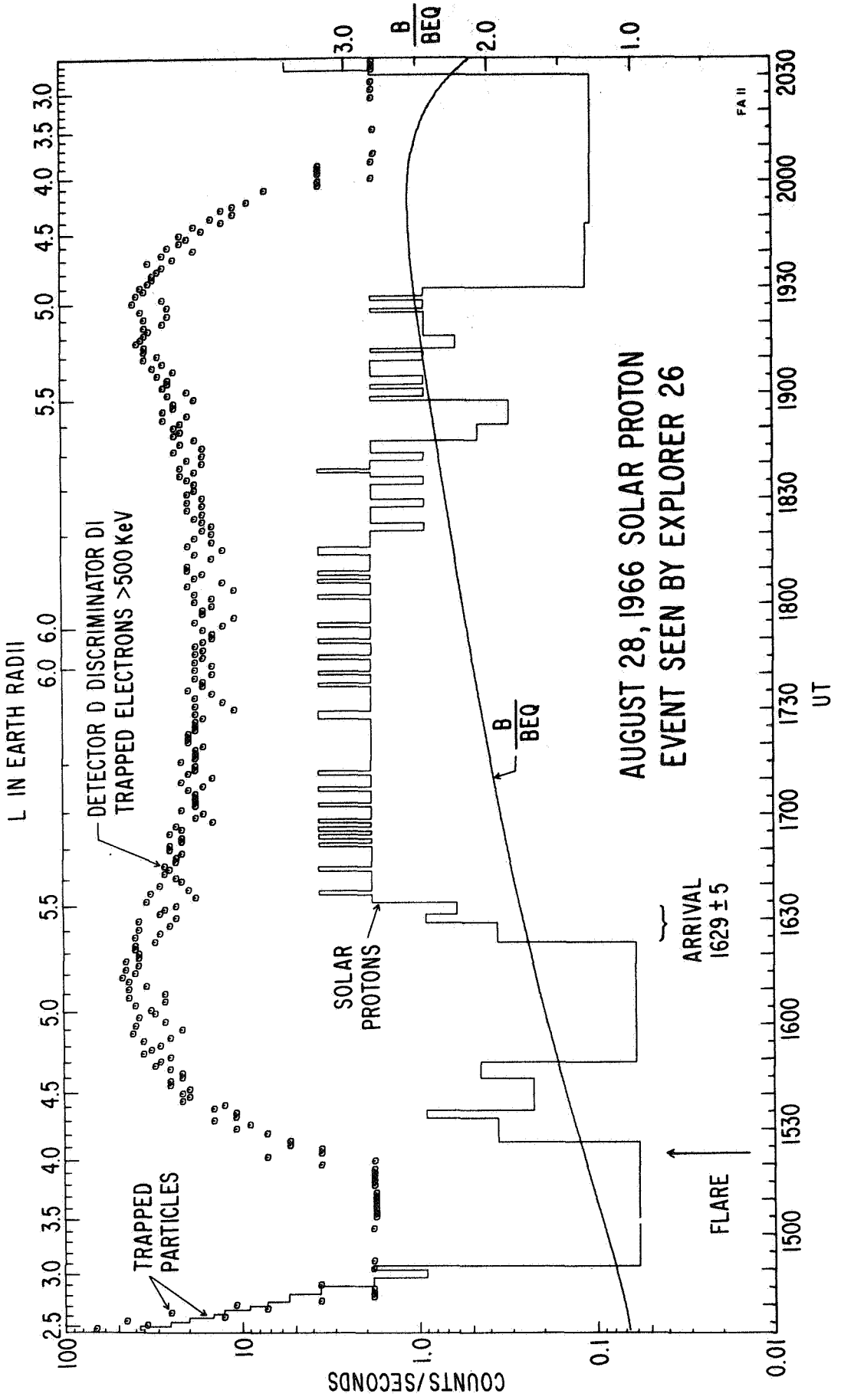
AUGUST 28, 1966 SOLAR PROTON
EVENT SEEN BY EXPLORER 26
DETECTOR D DISCRIMINATOR DI
TRAPPED ELECTRONS >500 KeV
TRAPPED
PARTICLES
SOLAR
PROTONS
ARRIVAL
1629 ± 5
FLARE
B/BEQ
L IN EARTH RADII
COUNTS/SECONDS
UT
FA II

Figure 5

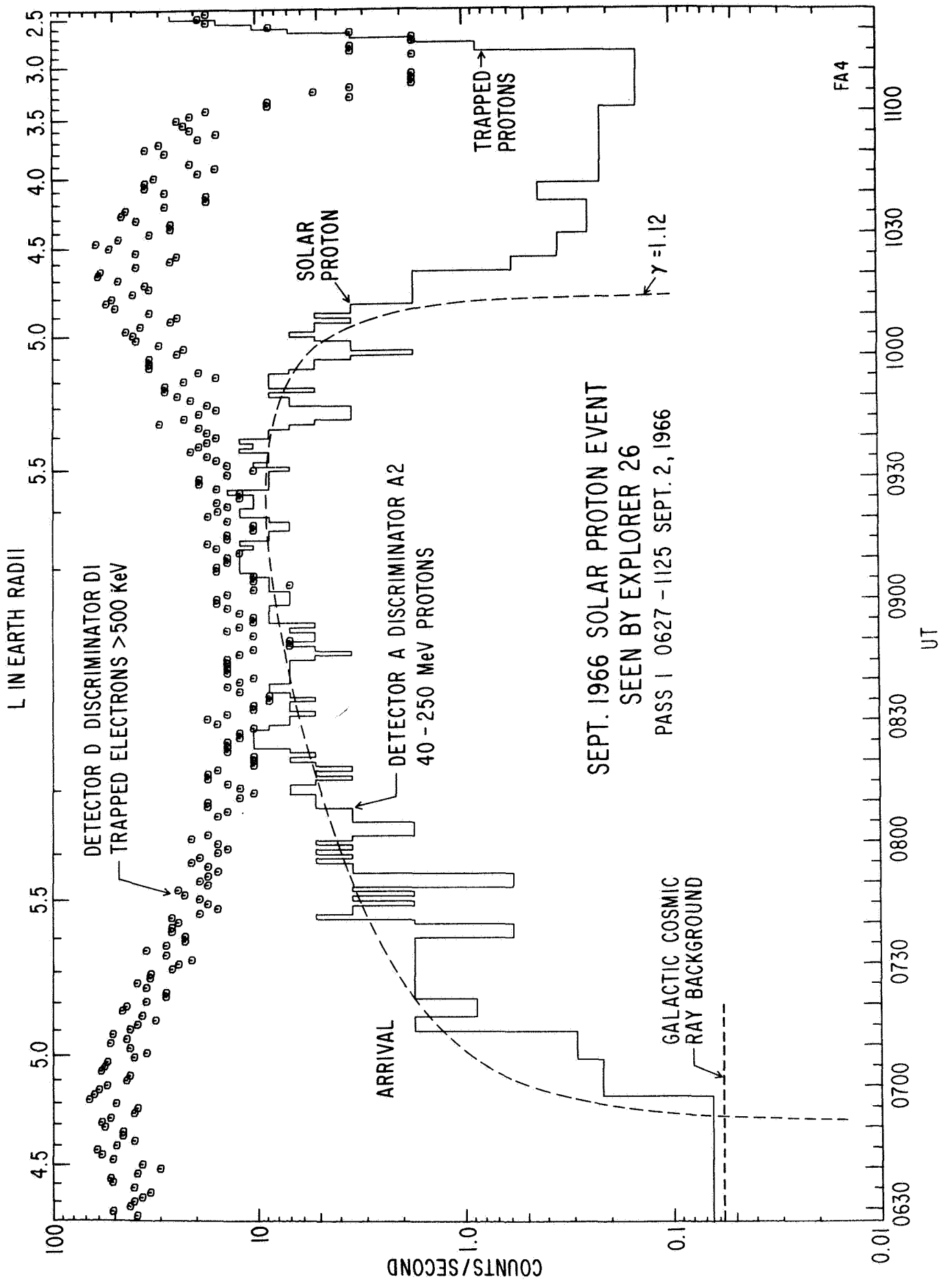
L IN EARTH RADII
DETECTOR D DISCRIMINATOR D1
TRAPPED ELECTRONS >500 KeV
DETECTOR A DISCRIMINATOR A2
40 - 250 MeV PROTONS
SOLAR PROTON
TRAPPED PROTONS
ARRIVAL
GALACTIC COSMIC RAY BACKGROUND
γ =1.12
SEPT. 1966 SOLAR PROTON EVENT
SEEN BY EXPLORER 26
PASS I 0627 - 1125 SEPT. 2, 1966
FA4
COUNTS/SECOND
UT

Figure 6

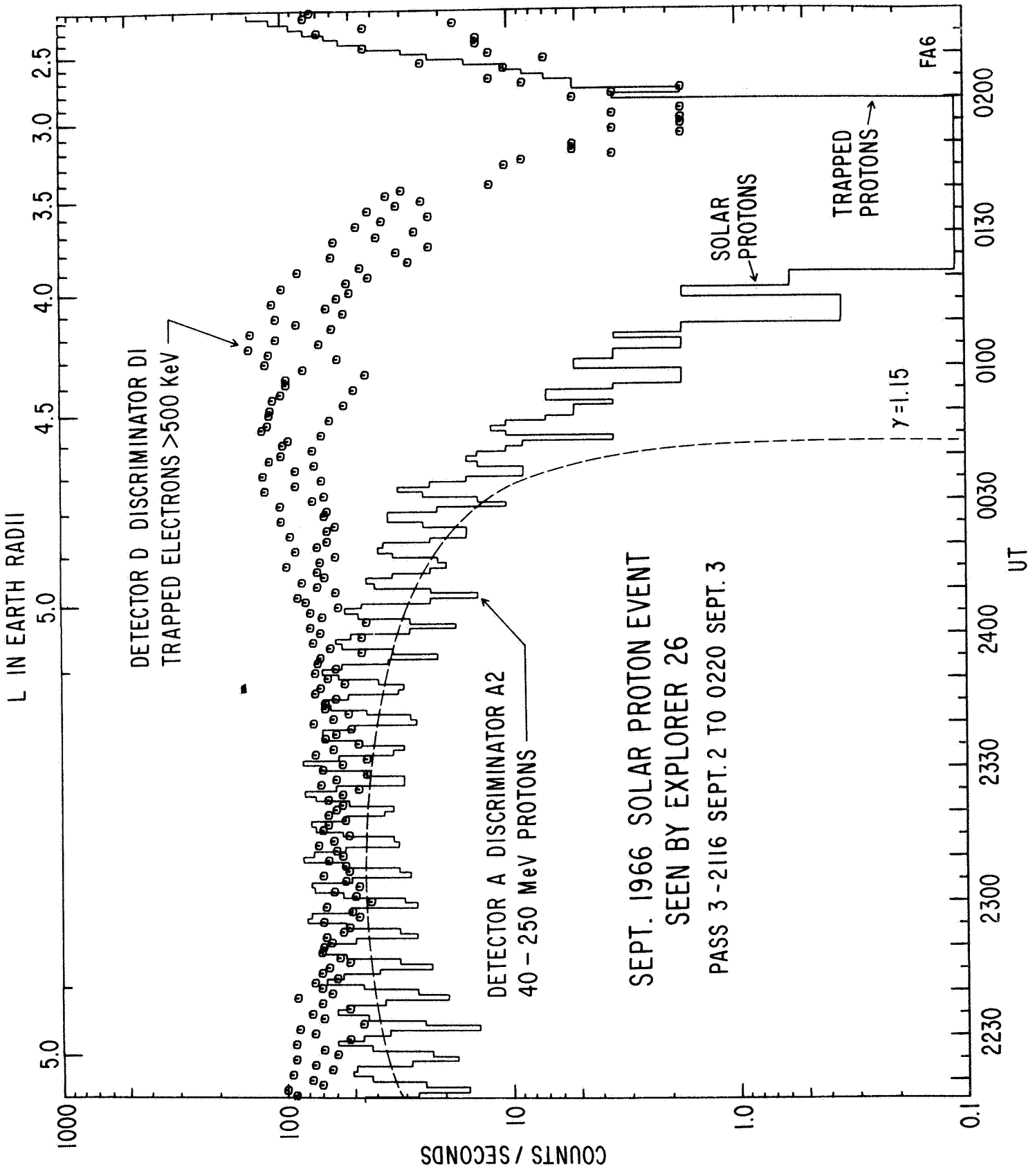
L IN EARTH RADII
5.0
4.5
4.0
3.5
3.0
2.5
5.0
DETECTOR D DISCRIMINATOR DI
TRAPPED ELECTRONS >500 KeV
DETECTOR A DISCRIMINATOR A2
40 – 250 MeV PROTONS
SEPT. 1966 SOLAR PROTON EVENT
SEEN BY EXPLORER 26
PASS 3 -2116 SEPT. 2 TO 0220 SEPT. 3
SOLAR PROTONS
TRAPPED PROTONS
FA6
γ=1.15
1000
100
10
1.0
0.1
COUNTS / SECONDS
2230
2300
2330
2400
0030
0100
0130
0200
UT

Figure 7

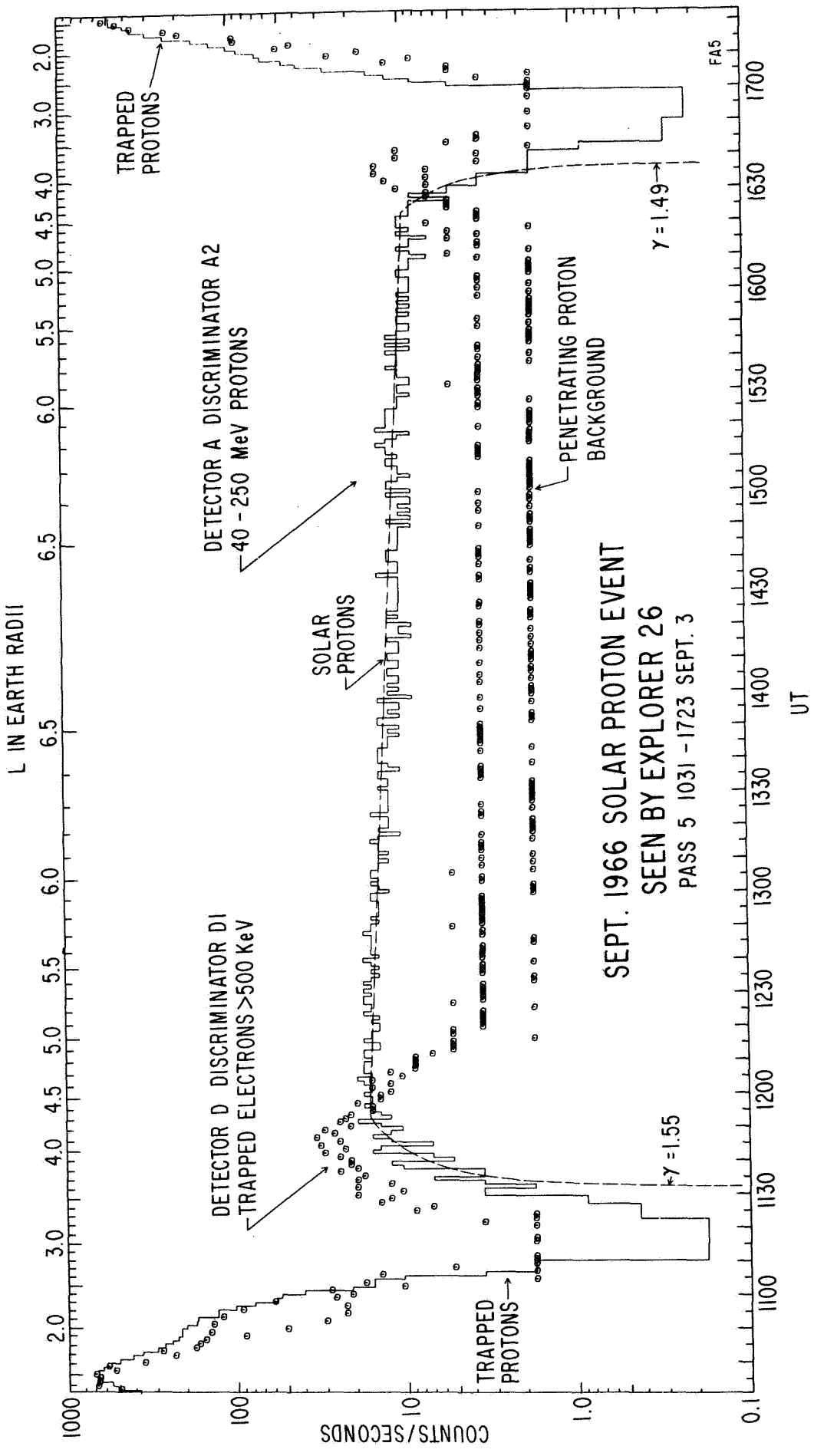
SEPT. 1966 SOLAR PROTON EVENT
SEEN BY EXPLORER 26
PASS 5 1031 - 1723 SEPT. 3
DETECTOR A DISCRIMINATOR A2
40 - 250 MeV PROTONS
DETECTOR D DISCRIMINATOR D1
TRAPPED ELECTRONS >500 KeV
TRAPPED PROTONS
SOLAR PROTONS
PENETRATING PROTON BACKGROUND
γ = 1.49
γ = 1.55
TRAPPED PROTONS
L IN EARTH RADII
UT
COUNTS/SECONDS
FA5

Figure

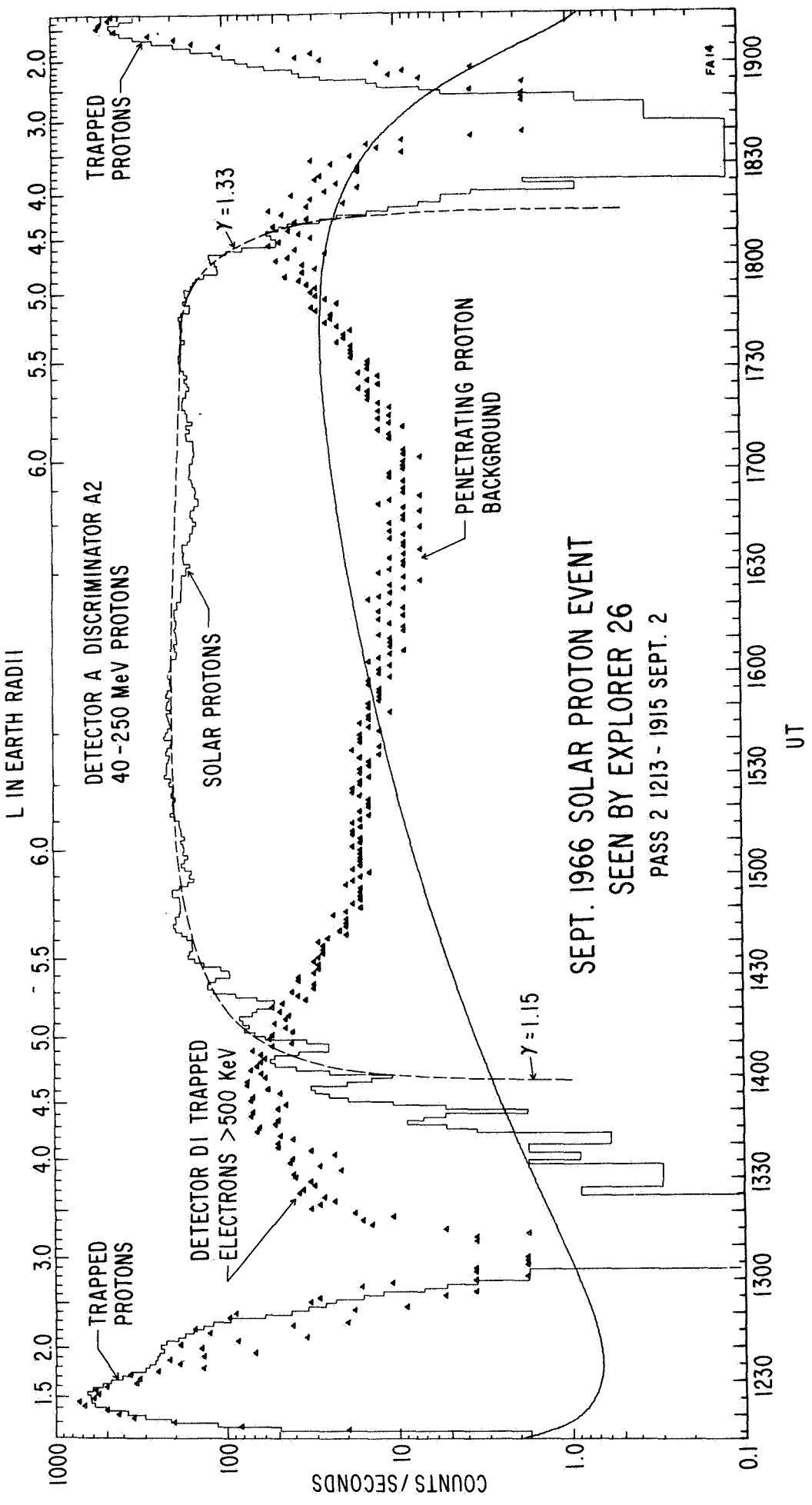
SEPT. 1966 SOLAR PROTON EVENT
SEEN BY EXPLORER 26
PASS 2 1213 - 1915 SEPT. 2
TRAPPED PROTONS
DETECTOR A DISCRIMINATOR A2
40 -250 MeV PROTONS
SOLAR PROTONS
γ = 1.33
PENETRATING PROTON BACKGROUND
DETECTOR DI TRAPPED ELECTRONS >500 KeV
γ = 1.15
TRAPPED PROTONS
L IN EARTH RADII
COUNTS / SECONDS
UT
FA14

Figure

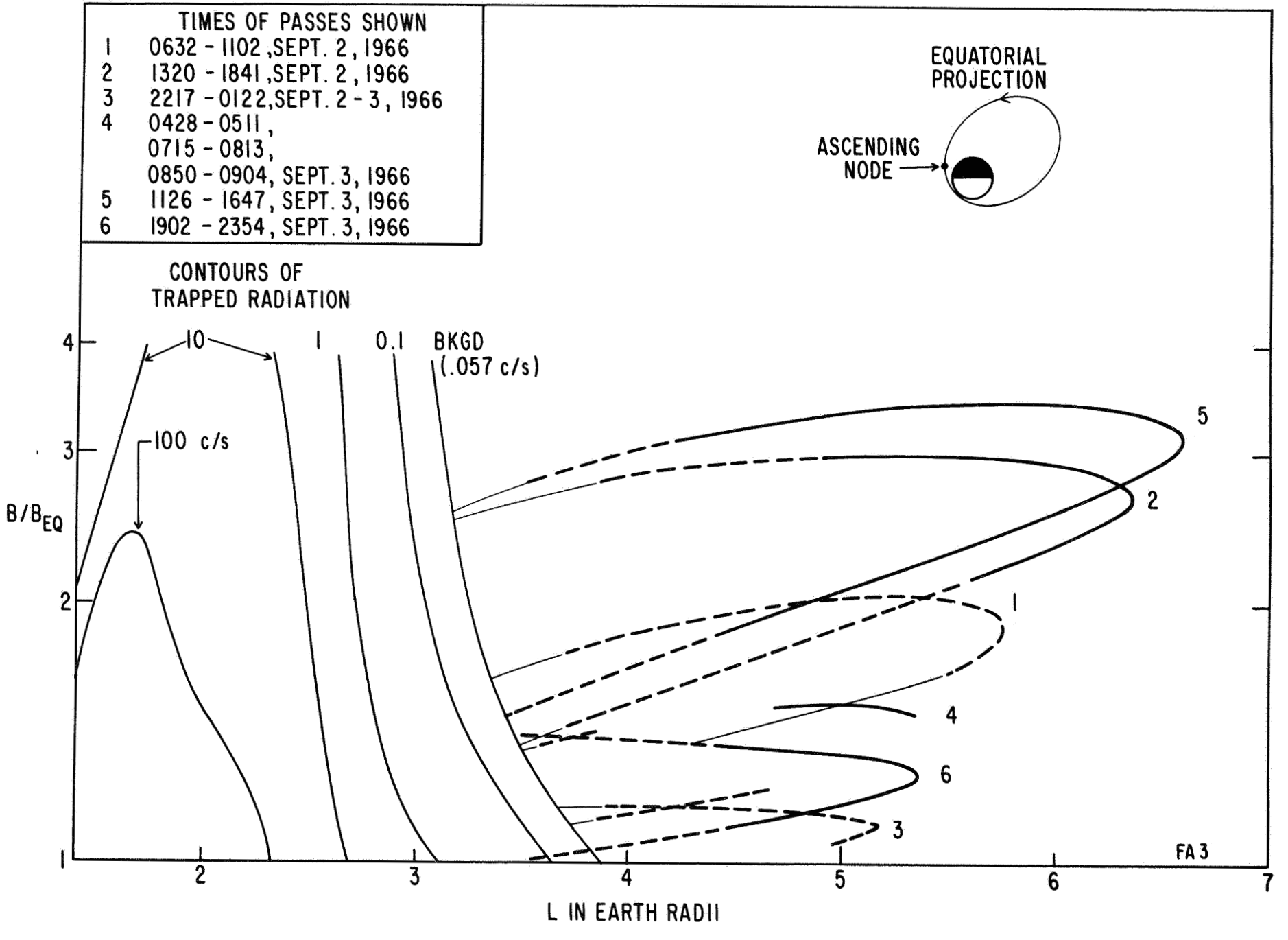
TIMES OF PASSES SHOWN
1 0632 - 1102, SEPT. 2, 1966
2 1320 - 1841, SEPT. 2, 1966
3 2217 - 0122, SEPT. 2 - 3, 1966
4 0428 - 0511,
0715 - 0813,
0850 - 0904, SEPT. 3, 1966
5 1126 - 1647, SEPT. 3, 1966
6 1902 - 2354, SEPT. 3, 1966
EQUATORIAL PROJECTION
ASCENDING NODE
CONTOURS OF TRAPPED RADIATION
10
1
0.1
BKGD (.057 c/s)
100 c/s
B/B_EQ
L IN EARTH RADII
FA 3

Figure 1

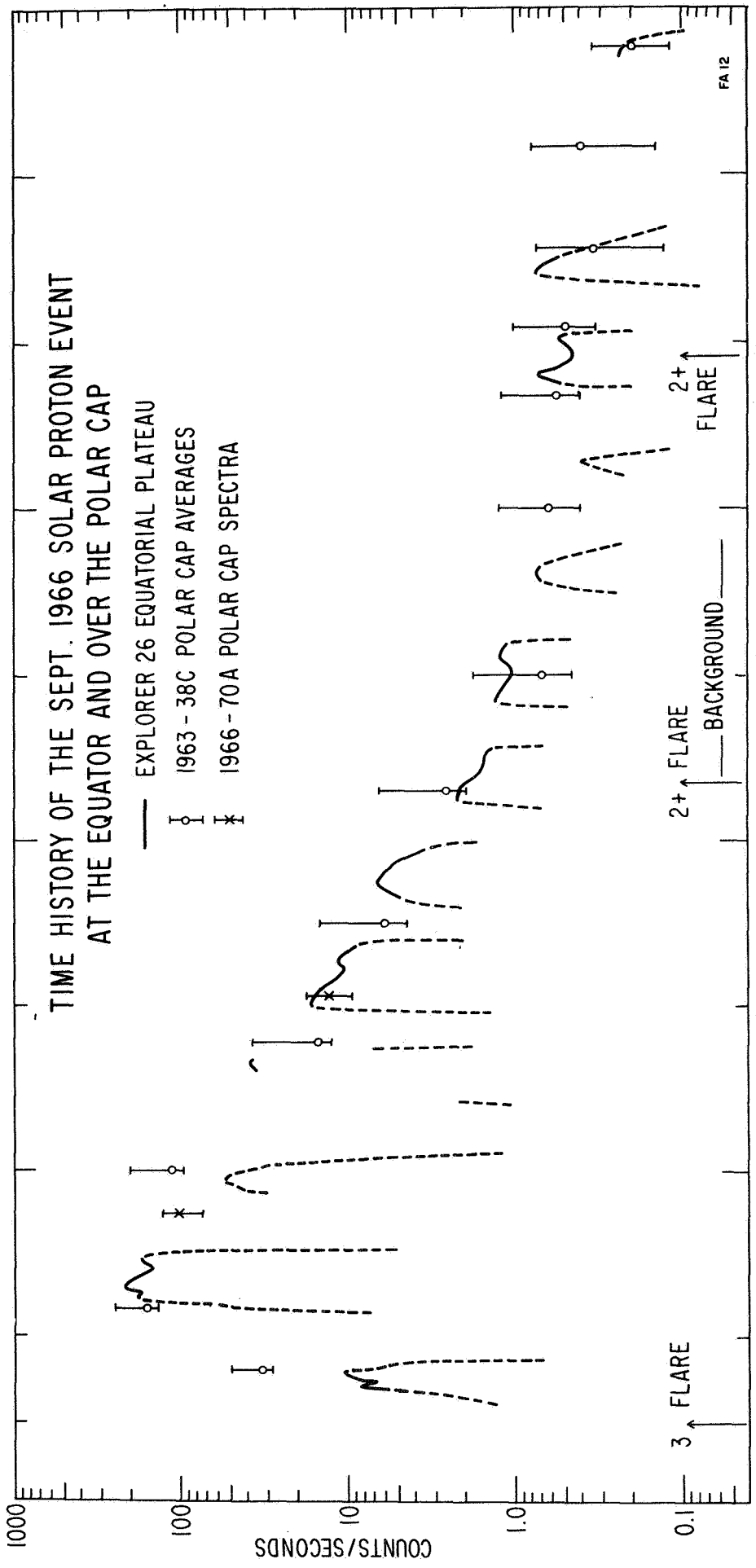
TIME HISTORY OF THE SEPT. 1966 SOLAR PROTON EVENT
AT THE EQUATOR AND OVER THE POLAR CAP
EXPLORER 26 EQUATORIAL PLATEAU
1963 - 38C POLAR CAP AVERAGES
1966 - 70A POLAR CAP SPECTRA
FA 12
COUNTS/SECONDS
1000
100
10
1.0
0.1
9/2/66
9/3/66
9/4/66
9/5/66
3 FLARE
2+ FLARE
BACKGROUND
2+ FLARE

Figure 11

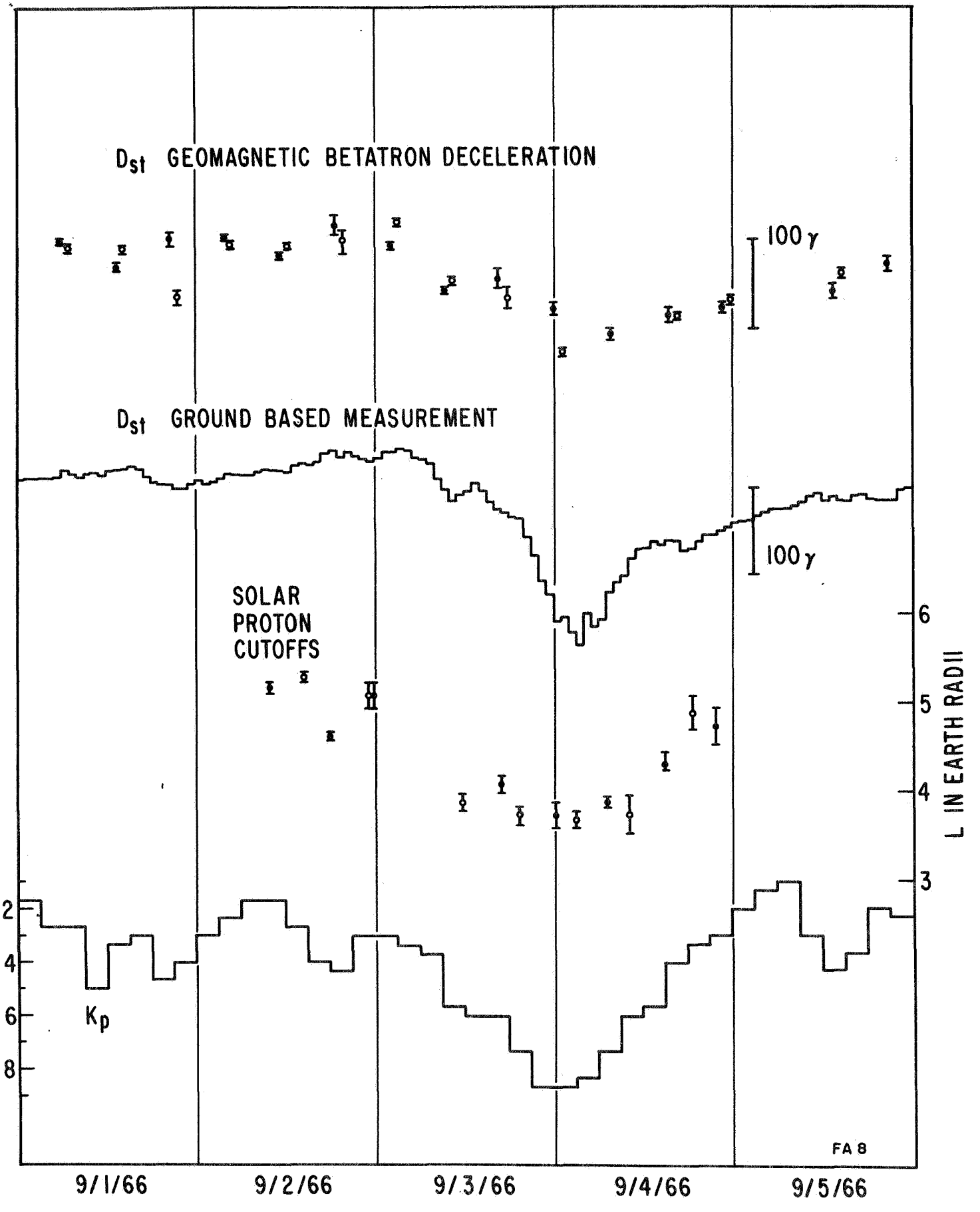
D_{st} GEOMAGNETIC BETATRON DECELERATION
100 γ
D_{st} GROUND BASED MEASUREMENT
100 γ
SOLAR
PROTON
CUTOFFS
Kp
2
4
6
8
3
4
5
6
L IN EARTH RADII
FA 8
9/1/66
9/2/66
9/3/66
9/4/66
9/5/66

Figure 12

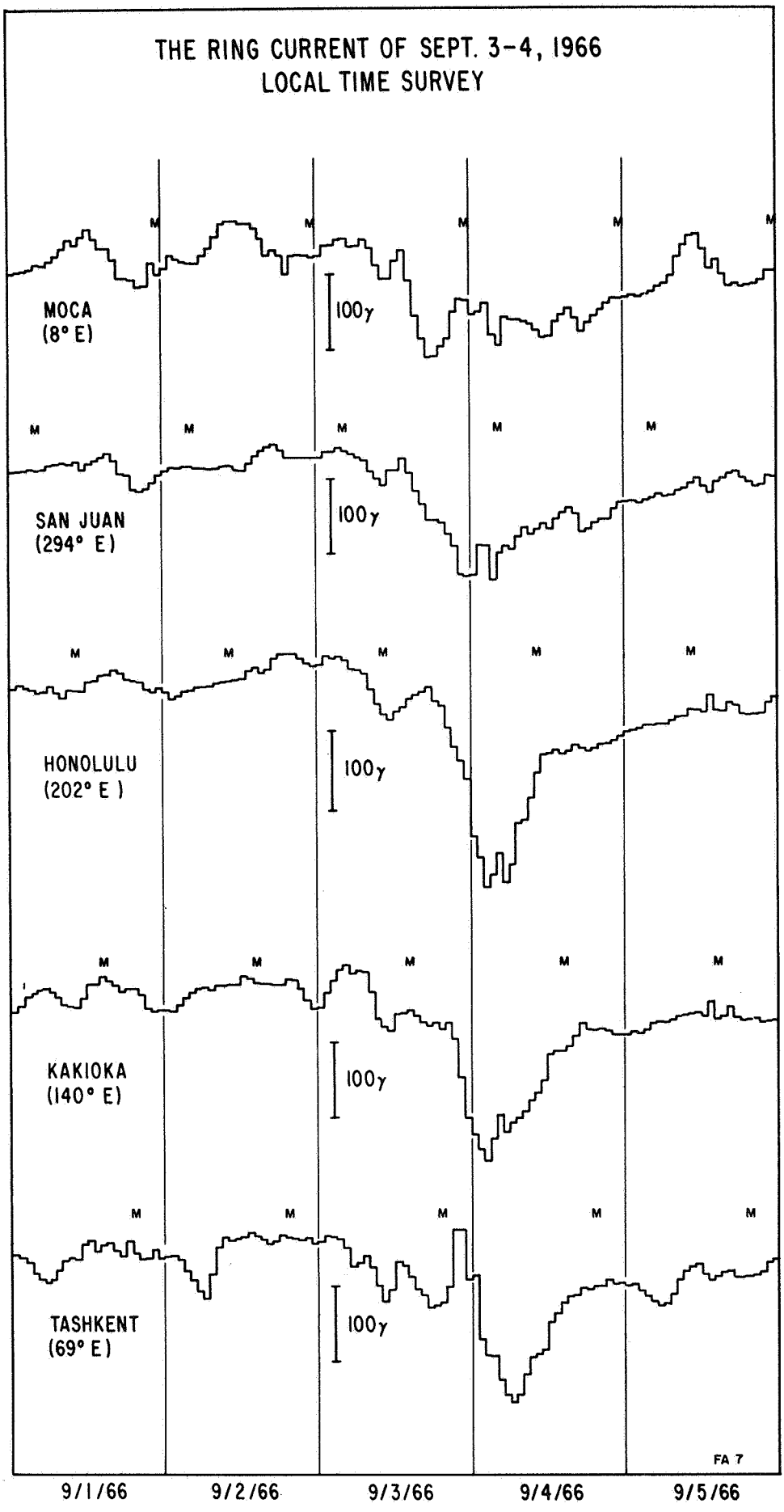
THE RING CURRENT OF SEPT. 3-4, 1966
LOCAL TIME SURVEY
MOCA
(8° E)
100γ
SAN JUAN
(294° E)
100γ
HONOLULU
(202° E)
100γ
KAKIOKA
(140° E)
100γ
TASHKENT
(69° E)
100γ
FA 7
9/1/66
9/2/66
9/3/66
9/4/66
9/5/66

Figure 13

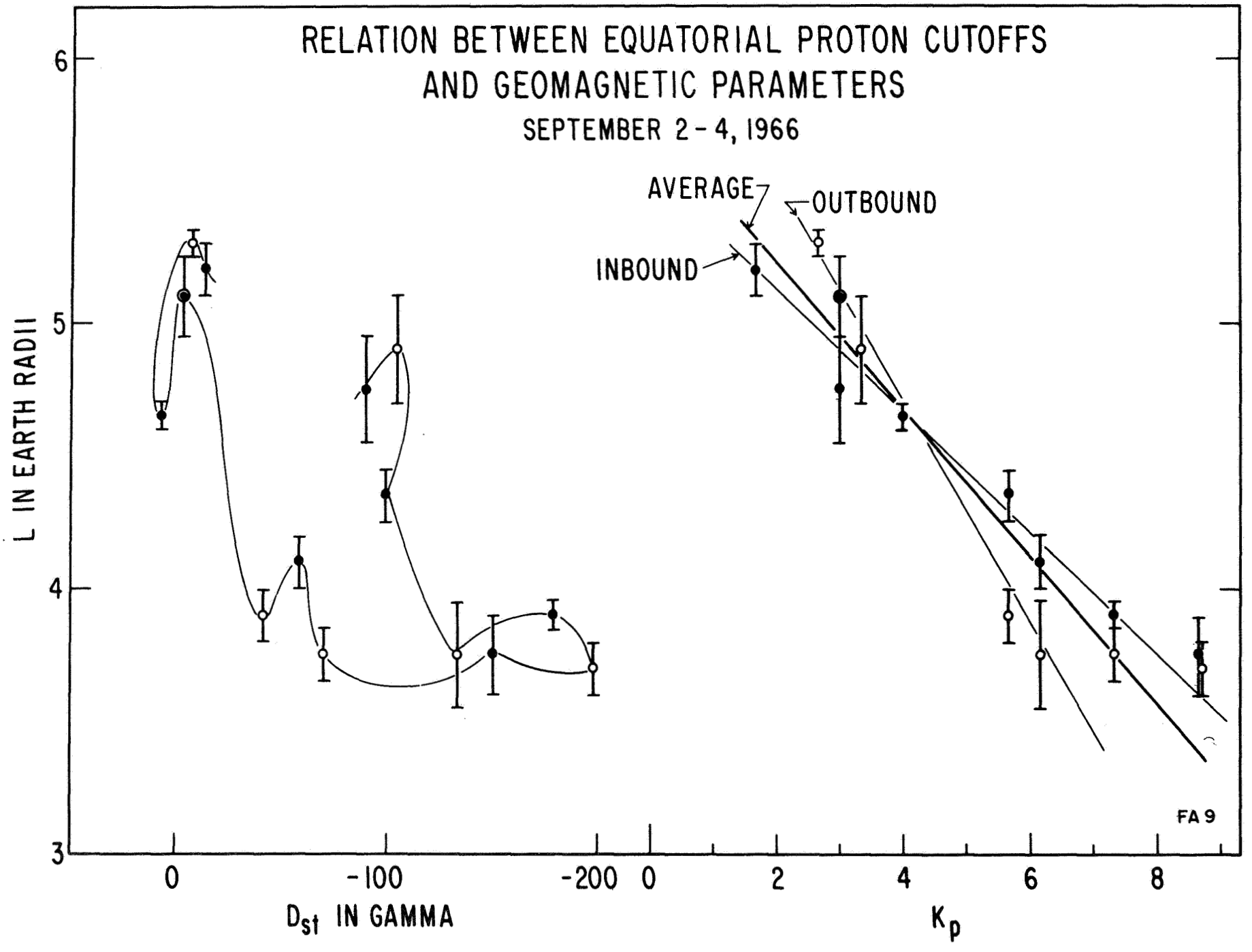
RELATION BETWEEN EQUATORIAL PROTON CUTOFFS
AND GEOMAGNETIC PARAMETERS
SEPTEMBER 2 - 4, 1966
AVERAGE
OUTBOUND
INBOUND
L IN EARTH RADII
6
5
4
3
0
-100
-200
D_{st} IN GAMMA
0
2
4
6
8
K_p
FA 9

Figure

APPENDIX

EQUATORIAL CUTOFFS WITH AN AXIALLY SYMMETRIC RING CURRENT

In this appendix we develop formulas, valid in the equatorial plane of an azimuthally symmetric magnetosphere, for the cutoff altitude of cosmic ray protons in the energy range measured by Explorer 26. We then study the theoretical effect of turning on a symmetrical ring current and demonstrate that, for a reasonable model of the magnetosphere and for almost any model of a ring current, its effect is to raise the cutoff altitude. We conclude that the data taken by Explorer 26 cannot be explained by any sort of symmetric ring current. This problem is, of course, a specialization of the Störmer problem; however, by restricting our consideration to the equatorial plane, we are able to generalize our magnetic field model.

Take a cylindrical coordinate system in which the magnetic field is everywhere parallel to $\hat{z}$ and $\hat{\varphi}$ is positive eastbound. A suitable and general magnetic vector potential is

$$\vec{A}(r) = \hat{\varphi} \frac{1}{r} \int_{\infty}^{r} r \, B_z(r) \, dr$$

The integral in this formula is all we will give to describe the ring current in many of our results. Labeling it $\Phi(r)$, we can use the divergence-free property of $\vec{B}$ to write

$$\Phi(r) \equiv \int_{\infty}^{r} r \, B_z(r) \, dr = \int_{o}^{r} r \, B_z(r) \, dr$$

The Lagrangian is

$$\mathcal{L} = 1/2\ mv^2 + e/c\ \vec{A} \cdot \vec{v}$$

where the symbol m stands for the relativistic mass

$$m_o / \sqrt{1 - v^2/c^2}$$

and is a constant. The Euler-Lagrange equation in the cyclic coordinate φ gives

$$mr^2\ \dot{\varphi} + e/c\ \Phi(r) = -2\ mv\gamma \qquad (A1)$$

Following Ray we have set the integration constant to $-2\ mv\gamma$. The parameter γ is an initial condition and will be important to the discussion. It has the dimensions of length, and if Φ vanishes at infinity, 2γ is seen to be the impact parameter of a cosmic ray's initial trajectory. It is positive for a proton aimed to the west of the earth. From the conservation of energy we have

$$1/2\ mv^2 = 1/2\ m\ \dot{r}^2 + V(r)$$

where the fictitious radial potential energy, V(r), is given by

$$V(r) = m/2 \left[2\gamma\ v/r + \frac{e}{mcr}\ \Phi(r) \right]^2 \qquad (A2)$$

This corresponds to the expression in classical Störmer theory that determines the zones of allowed $(E - V(r) > 0)$ and forbidden $(E - V(r) < 0)$ motion. Clearly $E = V(r)$ defines the cutoff points of allowed motion where the particles have no radial velocity.

Illustration for a Dipole Field

These features are a recognizable part of Störmer's solution if the formula for a dipole field, $-M/r$, is used for Φ. $r^4 (E - V(r))$ is now a fourth degree polynomial and the limits of allowed motion are the roots, given by

$$r_1 = -\gamma + \sqrt{\gamma^2 + 1}$$

$$r_2 = +\gamma - \sqrt{\gamma^2 - 1}$$

$$r_3 = +\gamma + \sqrt{\gamma^2 - 1}$$

From here on the unit of length is the customary Störmer unit

$$C_{st} = \sqrt{\frac{e\,M}{mvc}}$$

There is a fourth root which is not physical as it is negative for all γ. Also r_2 and r_3 become non-physical if the initial condition satisfies the inequality

$$\gamma < 1 \qquad \text{(A3)}$$

The smallest physical root is always r_1, and the way to lower this cutoff is to raise γ. However, as the roots r_2 and r_3 interpose a forbidden zone between infinity and r_1 when r_2 and r_3 are real, the cosmic ray that penetrates deepest is that one with maximum γ subject to condition A3. The cutoff for this particle is $(\sqrt{2} - 1)\, C_{st}$.

The Cutoff in a General Field

To make a general model of the real field take a dipole plus an unspecified perturbation in (A2):

$$\Phi(r) = -M/r + \Delta\Phi(r)$$

Now $r^4 (E - V(r))$ is not generally a polynomial, but barring changes in topology, the cutoff will once again be determined by the maximum γ for which a particle from infinity can reach the innermost root. The forbidden zone shrinks to a single gate point when $V(r) = E$ and $\frac{dV(r)}{dr} = 0$, and the solution of these simultaneous equations determines

r_g, the position of the gate point, and γ_g, the critical initial condition for a particle to reach the gate. Physically, the gate is the distance at which a particle whose rigidity is implicit in C_{st} has a radius of curvature equal to r_g; ie, the particle can describe a circle of radius r_g with the earth at the center. A particle which is initially aimed farther away from the earth ($\gamma > \gamma_g$) experiences smaller fields and is not deflected that close. A particle aimed slightly closer ($\gamma \lesssim \gamma_g$) hooks inward and executes a loop or loops below r_g. Minimum cutoff is the nadir of this loop, and it can be found by substituting γ_g into the cutoff equation $E = V(r)$ and solving for the innermost root r_c. The result is

$$r_c = -\gamma_p + \sqrt{\gamma_p^2 + 1} \tag{A4}$$

where

$$\gamma_p = \gamma_g + \frac{1}{2M} \Delta \Phi (r_c) \tag{A5}$$

As before the cutoff varies inversely as γ_p, and we can determine the direction in which the cutoff will change by assessing the perturbation's effect on γ_p. Using the solution for γ_g and the definition of Φ :

$$\gamma_p = \frac{1 - \frac{1}{2M} r_g \Delta B (r_g)}{\sqrt{1 - \frac{1}{M} r_g \Delta B (r_g)}} - \frac{1}{2M} (\Delta \Phi (r_g) - \Delta \Phi (r_c))$$

To first order in $\frac{r_g}{M} \Delta B (r_g)$

$$\gamma_p \approx 1 - \frac{1}{2M} (\Delta \Phi (r_g) - \Delta \Phi (r_c))$$

where it is worth pointing out that

$$\Delta \Phi (r_g) - \Delta \Phi (r_c) = \int_{r_c}^{r_g} r \Delta B(r) \, dr$$

Using this result we can assess the change in cutoff altitude with a minimum of information about the field perturbation.

Infinite Dipole Field Plus a Ring Current

As a first example consider a ring current superimposed on an infinite dipole field. The gate point of the unperturbed field is one Störmer length from the origin, which is 15 to 9 R_E over our detector's energy range and is 12 R_E for a typical (90 MeV) particle. At this distance ΔB is small and positive, increasing r_g. By measurement r_c is between 3 and 5 R_E. As this is near the seat of the ring current, assuredly the quantity $\Delta \Phi (r_c)$ is more negative than $\Delta \Phi (r_g)$. Alternatively one can say that the magnetic flux from the ring current, integrated from r_c to r_g, is positive (northward). The effect is to decrease γ_p and so to raise r_c. Thus can the promised result be obtained with practically no information required on the ring current.

Magnetosphere with Added Ring Current

In the previous model the gate point was found to be at about 12 R_E. This is bad, because we know that the magnetosphere is actually bounded by surface currents and this point is in interplanetary space where, in our symmetric approximation, there is no field. Obviously it is nonsense to talk about a gate point where the field is zero. Therefore we wish to make a model of the magnetosphere which includes

boundary currents and to investigate the change a ring current will produce when added to this model.

A spherical bounded magnetosphere can be obtained by constraining the surface currents to produce a uniform northward $\Delta B = 2M/r_b^3$ everywhere inside a sphere of radius r_b. Then the boundary-current field outside r_b will be dipolar and will cancel the primary dipole field to produce the null field of interplanetary space. To avoid discontinuities the surface current is given a small but finite thickness ϵ. The gate point is found easily by observing that, to deflect a particle, r_g must be below $r_b + \epsilon$; but a particle for which $C_{st} > r_b / \sqrt{3}$ has a radius of curvature less than r anywhere at or below r_b. As this includes the rigidity range of our experiment, a detectable particle that just circles the earth at height r_g is restricted to

$$r_b < r_g < r_b + \epsilon$$

Using $\Phi(r_g) = 0$ in (A1),

$$\gamma_g = r_{g/2} \approx r_{b/2}$$

Now (A5) gives

$$\gamma_p = \frac{r_b}{2} + \frac{1}{2M} \Delta \Phi (r_c)$$

and again (A4) is the cutoff distance.

When a ring current is introduced the total perturbation can be written as $\Delta \Phi'$ and the respective parameters as r_b', γ_p', and r_c'. The change in γ_p is given by

$$\Delta \gamma_p = \gamma_p' - \gamma_p = \tfrac{1}{2}(r_b' - r_b) + \frac{1}{2M} (\Delta \Phi'(r_c') - \Delta \Phi (r_c)) \quad (A6)$$

Now, if the magnetospheric boundary remains fixed, γ_p must decrease and r_c increase, because $\Delta \Phi'(r_c')$ is a substantial negative quantity. This is more convincing if $\Delta \Phi$ is written as a sum of boundary and ring current terms:

$$\Delta \Phi = \Delta \Phi_r + \Delta \Phi_b = \Delta \Phi_r + \frac{M}{r_b^3} r^2$$

Then $\Delta \gamma_p$ becomes

$$\Delta \gamma_p = \frac{1}{2r_b^3} (r_c'^2 - r_c^2) + \frac{1}{2M} \Delta \Phi_r'(r_c')$$

If we assume what we are trying to disprove, namely that $r_c' < r_c$, then both terms are negative, $\Delta \gamma_p < 0$, and $r_c' > r_c$, in contradiction to the assumption. Thus if r_b remains fixed the cutoff is raised, again with practically no restriction on the ring current.

In order to include possible movement of the boundary we must introduce two more variables representing the factors that would compress or inflate the magnetosphere. Tending to compress the boundary is the solar wind pressure p. Acting in the opposite direction is an increase in the magnetic field pressure inside the boundary caused by the ring current plus an augmented boundary current. It is reasonable to assume that, as far out as the boundary, the ring current field is a dipolar M_r'/r^3. It is canceled in interplanetary space by an increase in the boundary current moment, $M' = M + M_r'$. Equation A6 becomes

$$\Delta \gamma_p = \frac{r_b}{2} \left[(p/p')^{1/6} (M'/M)^{1/3} - 1 \right]$$

$$+ \frac{r_c^2}{2r_b^3} \left[\left(\frac{r_c'}{r_c} \right)^2 \left(\frac{p'}{p} \right)^{\frac{1}{2}} - 1 \right]$$

$$+ \frac{1}{2M} \Delta \Phi_r' (r_c')$$

The polarity of $\Delta \gamma_p$ is decided by a competition between term 3 above, which is negative, and term 1, which may be positive. Term 2 is small, but if necessary it can be dealt with as before by assuming $r_c' < r_c$ and demonstrating the contradiction. As an upper limit to $\Delta \Phi' (r_c')$ take $- M_r/r_b'$, so that term 3 is less than

$$\frac{1}{2 r_b'} \frac{M'}{M} - 1$$

Comparison with term 1 shows that $\Delta \gamma_p < 0$ and therefore the cutoff is raised as before.

Throughout this entire discussion we have taken pains to assume as little as possible about the shape of the ring current field. Therefore we believe that the result is inescapable: no symmetric field and ring current could have lowered the cutoff altitude of the solar protons observed by Explorer 26.

Acknowledgment

I wish to express my gratitude to Dr. Carl McIlwain who suggested this study and made the Explorer 26 data available, and to the other experimenters, Dr. Carl Bostrom of the Johns Hopkins University Applied Physics Laboratory, Dr. George Paulikas of Aerospace Corporation, and Dr. John Gosling of the Los Alamos Scientific Laboratory, who cooperatively provided unpublished data for comparison. I have profited from discussions with the above and also with Dr. Herbert Sauer of ESSA. This work was supported in part by the National Aeronautics and Space Administration under contract NAS 5-3063 and grant NsG-538.

References

Akasofu, S.-I, W. C. Lin and J. A. Van Allen, The anomalous entry of low-rigidity solar cosmic rays into the geomagnetic field, J. Geophys. Res. 68, 5327-5338, 1963.

Anderson, K. A., R. Arnoldy, R. Hoffman, L. Peterson, and J. R. Winckler, Observations of low-energy solar cosmic rays from the flare of 22 August 1958, J. Geophys. Res. 64, 1133-1147, 1959.

Axford, W. I., Anisotropic diffusion of solar cosmic rays, Planet. Space Sci. 13, 1301-1309, 1965.

Bailey, D. K., Polar-cap absorption, Planet. Space Sci., 12, 495-541, 1964.

Behannon, K. W. and N. F. Ness, Magnetic storms in the earth's magnetic tail, J. Geophys. Res. 71, 2327-2351, 1966.

Bostrom, C. O., private communication, 1967.

Bryant, D. A., T. L. Cline, U. D. Desai, and F. B. McDonald, Explorer 12 observations of solar cosmic rays and energetic storm particles after the solar flare of September 28, 1961, J. Geophys. Res. 67, 4983-5000, 1962.

Burlaga, Leonard Francis, Anisotropic diffusion of solar cosmic rays, J. Geophys. Res. 72, 4449-4466, 1967.

Fibich, Moshe and Phillip B. Abraham, On the propagation and diffusion of solar protons, J. Geophys. Res. 70, 2475-2484, 1965.

Friedland, Allan B., Trapped radiation shells and cosmic-ray cutoffs in models of the magnetosphere, J. Geophys. Res. 72, 1495-1511, 1967.

References (Continued)

Gall, Ruth, Jaime Jiménez and Lucila Camacho, On the channelling effect of the magnetospheric tail on the motion of low energy cosmic rays, Instituto de Geofisíca, Univ. Nacional Autónoma de México and Com. Nacional de Energía Nuclear Preprint (Submitted to J. Geophys. Res., March 1967)

Gosling, John, Private Communication, February 23, 1967.

Kahler, S. W., J. H. Primbsch, and K. A. Anderson, Energetic protons from the solar flare of March 24, 1966, Solar Physics 2, 179-191, 1967.

Krimigis, S. M., Interplanetary diffusion model for the time behavior of intensity in a solar cosmic ray event, J. Geophys. Res. 70, 2943-2960, 1965.

Krimigis, S. M. and J. A. Van Allen, Observations of the February 5-12, 1965, solar particle event with Mariner 4 and Injun 4, J. Geophys. Res. 72, 4471-4486, 1967.

Lin, W. C. and J. A. Van Allen, Observation of solar cosmic rays from October 13, 1959 to February 17, 1961 with Explorer VII, Rendiconti Della Scuola Internazionale Di Fisica, Enrico Fermi, XXIV Corso, Academic Press, N.Y., London, 1964.

McIlwain, C. E., Measurements of trapped electron intensities made by the Explorer XV satellite, Radiation Trapped in the Earth's Magnetic Field, 593-609, McCormac, Billy M., ed., D. Reidel Publishing Company, Dordrecht-Holland, 1966.

McIlwain, Carl E., Ring current effects on trapped particles, J. Geophys. Res. 71, 3623-3628, 1966.

References (Continued)

Ogilvie, K. W., D. A. Bryant, and L. R. Davis, Rocket observations of solar protons during the November 1960 events, 1, J. Geophys. Res. 67, 929-937, 1962

Paulikas, G. A., J. B. Blake and S. C. Feden, Low energy cosmic ray cutoffs: diurnal variations and pitch angle distributions, J. Geophys. Res. 73, 87-96, 1968.

Parker, E. N., Interplanetary Dynamical Processes, Interscience Publishers, New York, 1963.

Pieper, G. F., A. J. Zmuda, C. O. Bostrom, and B. J. O'Brien, Solar protons and magnetic storms in July 1961, J. Geophys. Res. 67, 4959-4981, 1962.

Ray, Ernest C., On the motion of charged particles in the geomagnetic field, Annals of Physics, 24, 1-18, 1963.

Ray, Ernest C., Cosmic-ray cutoffs at high latitude, J. Geophys. Res. 69, 1737-1741, 1964.

Reid, G. C. and H. H. Sauer, The influence of the geomagnetic tail on low-energy cosmic-ray cutoffs, J. Geophys. Res. 72, 197-208, 1967.

Roederer, Juan G., On the adiabatic motion of energetic particles in a model magnetosphere, J. Geophys. Res. 72, 981-992, 1967.

Sauer, Herbert H. and Ernest C. Ray, On cosmic ray cutoffs, Annals of Physics 25, 135-142, 1963.

Stone, Edward C., Local time dependence of non-Störmer cutoff for 1.5-Mev protons in quiet geomagnetic field, J. Geophys. Res. 69, 3577-3582, 1964.

Van Allen, J. A. and Wei Ching Lin, Outer radiation belt and solar proton observations with Explorer VII during March-April 1960, J. Geophys. Res. 65, 2998-3003, 1960.